A PHOTOELASTIC STUDY OF STRESS DISTRIBUTION IN A SPUR GEAR TOOTH

by

Kuo Chang Wang

Thesis submitted to the Graduate Faculty of the
Virginia Polytechnic Institute
in candidacy for the degree of

MASTER OF SCIENCE

in

MECHANICAL ENGINEERING

APPROVED:

Director of Graduate Studies

Head of Department

Dean of Engineering

E. D. Harrison
Major Professor

August, 1954

Blacksburg, Virginia

TABLE OF CONTENTS

I. LIST OF FIGURES

II. LIST OF TABLES

III. NOTATION

Symbol	Definition
X, Y	Rectangular coordinates
n	Fringe order
θ	Isoclinic parameter
σ_x, σ_y	Normal stress components parallel to X- and Y-axis
τ_{xy}	Shearing stress component in rectangular coordinates
p	Maximum principal stress
q	Minimum principal stress
ϕ	Airy stress function
U	Harmonic function
f	Material fringe constant

IV. INTRODUCTION

With continued increase in the loading and peripheral speed of gears, the problem of the strength of gear teeth, which has so far not been successfully solved becomes more important and the necessity of a deeper study of the stress distribution for this case becomes more imperative.

To prevent breaking and excessive wear, a satisfactory gear tooth must possess a hard surface and a tough core. Hardness of certain metals, such as steel, is proportional to its tensile strength (1), toughness will, on the contrary, be sacrificed with an increase in hardness. Proper determination of these mutually affected factors requires the knowledge of stress distribution at points on the boundaries of a gear tooth as well as points within its interior region.

Stresses developed in the gear teeth are considered as plane stresses. Due to the complicated boundary conditions, a rigorous mathematical solution for this plane stress problem is very difficult, though not absolutely impossible. However certain experimental methods together with some numerical approximations for solving the equilibrium equations and the compatibility equation have been developed which will enable us to approach the problem with sufficient accuracy for all practical purposes.

As will be seen later, the photoelastic method, the shear difference method and the numerical iteration process for solving the Laplace's Equation are used in this investigation.

Numbers in parentheses refer to ~~refer to~~ references in the bibliography.

V. THE REVIEW OF LITERATURE

Wilfred Lewis, a pioneer in gear strength problem, first introduced his famous Beam Strength formula in 1892 (2). He considered a gear tooth as a cantilever beam, but he overlooked the factor of stress concentration and the factor of surface fatigue. These factors are of great importance to this problem. His formula, though widely used over the past 60 years, actually is not correct. The reason that it still gives satisfactory results in some cases is simply due to the use of large safety factors.

In 1922 - 1923, the photoelastic method was used by Professor E. G. Coker and his former student, Dr. Chakko (3), to solve the problem of gear stresses. They studied isoclinics, stress trajectories and the boundary stress of a gear tooth. They pointed out that a great variation in the contact stress exists due to the complicated curved boundaries.

In 1926, Timoshenko and Baud (4) investigated the stress concentration at the fillets of gear teeth by the photoelastic method and discussed the local stress at the surface of contact of two teeth in mesh by using the Herz Theory. They suggested the correction factors to modify the Lewis Formula and also proved that the calculated deflection of gear teeth is usually less than the inaccuracies inherent in the manufacture of gears.

In 1929, Baud and Peterson (5) made an investigation to compute analytically the load distribution among teeth in contact and to deter-

mine by photoelasticity some general stress relations for gears in which the number of teeth carrying the load varies. They concluded that increasing the contact ratio produces more favorable load and stress cycles.

P. H. Black (6) made a photoelastic investigation in 1936. He determined the stress concentration factors for spur gear teeth of Brown and Sharpe Form and the stresses around the keyway of the same gear blank.

In 1942, Dolan and Broghamer (7) conducted an extensive photoelastic study in which 105 Bakelite models, each of a single tooth, were made with different sizes, pressure angles, and fillet radii. These models were tested at different loading positions. The purposes were to determine a set of stress concentration factors and to study the relative effect when one of the variables changed.

In addition to the boundary stress, Dr. E. D. Harrison investigated the sub-surface stress of a 20-degree Full-Depth Involute gear tooth by using the photoelastic method. His work was for his doctorate thesis which was approved by the Purdue University in 1952.

VI. THE INVESTIGATION

A. Object of the Investigation

The object of this investigation is to determine the stress distribution in a 4-Pitch, 16-Tooth, 14½-Degree Composite Spur Gear Tooth. Both the boundary and subsurface stresses were studied.

In doing so, such results as the maximum stresses and stress concentration factor were also obtained.

B. Method of Approach

1. General Equation

The state of stress in a gear tooth is usually considered as two-dimensional. If expressed in Cartesian coordinates with the body force neglected, the two dimensional plane stresses must simultaneously satisfy:

a. The Equilibrium Equations

$$\frac{\partial \sigma_x}{\partial x} + \frac{\partial \tau_{xy}}{\partial y} = 0 \; ; \qquad \frac{\partial \sigma_y}{\partial y} + \frac{\partial \tau_{xy}}{\partial x} = 0$$

b. The Compatibility Equation

$$\left(\frac{\partial^2}{\partial x^2} + \frac{\partial^2}{\partial y^2}\right)\left(\sigma_x + \sigma_y\right) = 0$$

c. The Boundary Conditions

$$\bar{X} = l\sigma_x + m\tau_{xy} \; ; \qquad \bar{Y} = m\sigma_y + l\tau_{xy}$$

To obtain a solution of a two dimensional problem, the common procedure is to introduce the Airy function ϕ such that

$$\sigma_x = \frac{\partial^2 \phi}{\partial y^2} \quad ; \qquad \sigma_y = \frac{\partial^2 \phi}{\partial x^2} \quad ; \qquad \tau_{xy} = \frac{-\partial^2 \phi}{\partial x \partial y}$$

which evidently will satisfy the Equilibrium Equations. Substituting into the Compatibility Equation gives

$$\frac{\partial^4 \phi}{\partial x^4} + 2 \frac{\partial^4 \phi}{\partial x^2 \partial y^2} + \frac{\partial^4 \phi}{\partial y^4} = 0$$

Thus the problem is simply reduced to finding a solution of this equation subject to the boundary conditions. Unfortunately since the complicated boundary of a gear tooth is composed of straight lines and trochoidal and involute curves, it is too difficult, though not absolutely impossible, to find such a solution analytically.

2. The Shear Difference Method

The equilibrium equation,

$$\frac{\partial \sigma_x}{\partial x} + \frac{\partial \tau_{xy}}{\partial y} = 0$$

if written in difference form, will become

$$\frac{\Delta \sigma_x}{\Delta x} + \frac{\Delta \tau_{xy}}{\Delta y} = 0$$

hence $$(\sigma_x)_n = (\sigma_x)_{n-1} - \left(\frac{\Delta \tau_{xy}}{\Delta y} \right) \Delta x$$

where τ_{xy} and consequently $\Delta \tau_{xy}$ can be determined photoelasticially by the relation:

$$\tau_{xy} = \frac{p - q}{2} \sin 2\theta$$

The stress pattern and isoclinics respectively provide the value of (p - q) and θ involved.

At the free boundary one of the principal stresses, (p or q) vanishes, and therefore the initial value of $(\sigma_x)_o$ can be obtained

either by using Mohr's circle or from the relation:

$$\sigma_\theta = \frac{p+q}{2} + \frac{p-q}{2}\cos 2\theta$$

where $(p-q) = p$ or q, θ is also known. In this investigation, this relation was used.

Thus the Difference Equation may be completely solved. Though by the same procedure, we can find the corresponding σ_y, a much easier way is to calculate by the equation:

$$\sigma_y = \sigma_x \pm \sqrt{(p-q)^2 - 4\tau_{xy}^2}$$

Since the sum of the normal stresses on two mutually perpendicular planes is constant, i.e.

$$p + q = \sigma_x + \sigma_y = \text{Constant}$$

and since the stress pattern furnishes the value of $(p-q)$, we find p and q as soon as σ_x and σ_y for the same point are known.

3. Region of Investigation and its Boundary Values

Figure 1 shows the bourdaries enclosing the investigated area where the bending stresses are most critical.

Along the straight boundaries EF, GL, LK, HK, the stresses, σ_x and σ_y, p and q can be evaluated by the Shear Difference Method as outlined above. Along the curved boundaries, EG, FH, the stress pattern yields directly the values of p and q.

Of course the Shear Difference Method can be carried through to evaluate the stresses at every point inside the entire region to be investigated. However an alternative method as described below can also be used.

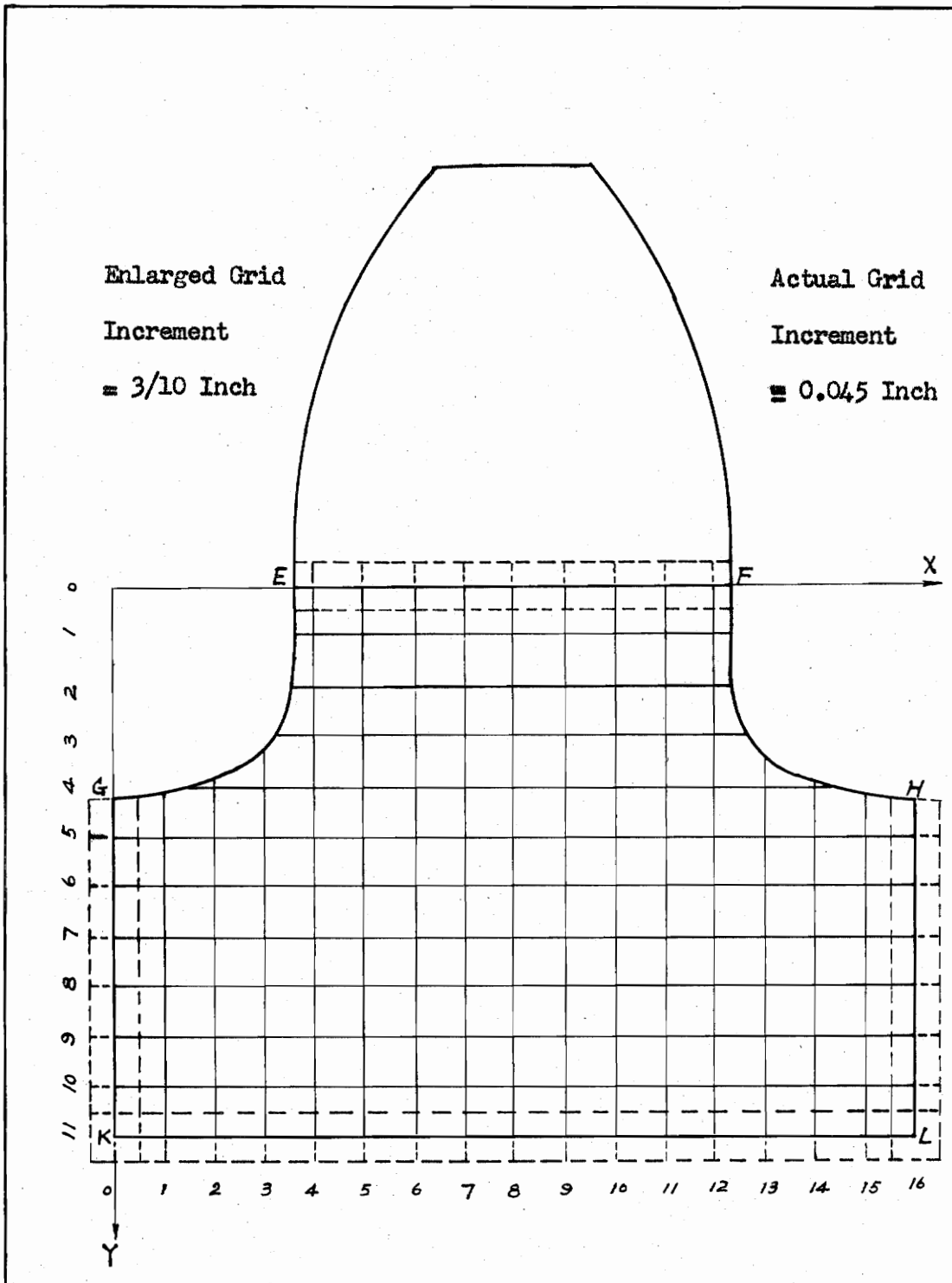

Fig. 1 - Boundaries and Grid Network

4. Laplace's Equation

As mentioned above, at every point of the region, the photoelastic stress pattern yields directly the value of (p-q), while the sum of p and q for that point is constant, i.e.

$$p + q = \sigma_x + \sigma_y = \text{Constant} = U(x,y)$$

Hence as long as the function U(x,y) can be determined, it will be easy to find the separate value for p and q, or σ_x and σ_y and then our problem is solved. (note that p, q, σ_x and σ_y all are functions of x and y).

To determine U(x,y), we rewrite the Compatibility equation:

$$\frac{\partial^2 U(x,y)}{\partial x^2} + \frac{\partial^2 U(x,y)}{\partial y^2} = 0$$

which is a Laplace's Equation in two dimensions.

A solution of Laplace's Equation is a Harmonic Function. The fundamental property of a harmonic function is formulated in Dirichlet's theorem (see Frocht's Photoelasticity Vol.I, p. 238 or books dealing with the Potential Theory) which states:

" For a given boundary Γ enclosing a region R to which the function applies, and for a specified boundary value on Γ, there exists only one solution of Laplace's equation for all points inside that region."

This means, in our case, that the sum of the principal stresses U is uniquely determined at every point within the region being investigated provided the boundary stresses are known.

Our problem now reduces to a boundary value problem. A rigorous

mathematical solution of the Laplace's Equation is possible only in cases where the boundaries are relatively simple. When the boundaries are complicated as in this case, it is difficult, if not absolutely, to find an analytical solution. However some numerical methods of solution have been developed which are sufficiently accurate for practical purposes.

5. Numerical Solution of Laplace's Equation

A numerical solution $U_o(x,y)$ of Laplace's equation at an arbitrary point O of the region R to which the function $U(x,y)$ applies must satisfy the Four-Point Influence Equation (see Frocht's Photoelasticity Vol. II, p.289 or Quarterly Applied Mathematics, Vil. II, July, 1944):

$$\left(\frac{1}{ac} + \frac{1}{bd}\right) U_o = \frac{1}{a(a+c)} U_a + \frac{1}{b(b+d)} U_b + \frac{1}{c(c+a)} U_c + \frac{1}{d(d+b)} U_d$$

where U_a, U_b, U_c, U_d are the value of the harmonic function $U(x,y)$ at four neighboring points $A(a,0)$, $B(0,b)$, $C(-c,0)$, and $D(0,-d)$.

In the case of an equally spaced network, the four point equation reduces to the Liebmann formula:

$$4U_o = U_a + U_b + U_c + U_d$$

The process of harmonization or adjustment to make the value of a harmonic function agree with the Four-Point equation at each point, as used in this investigation, is the Iterative Process. This is due to Dr. Frocht's suggestion((see his Photoelasticity Vol. II, p.286).

The smaller the increment of network and the more times the iteration, the more accurate the result. In this investigation, incre-

ment of 0.045 inch was used. Twelve iterations were performed.

C. The Apparatus and Model

1. The Apparatus

The group of experiments for this investigation was conducted at the Photoelasticity Laboratory of the Applied Mechanics Department, Virginia Polytechnic Institute. The apparatus used is shown in Figure 2 through 3 inclusive. It consists mainly of a standard polariscope, a loading machine and accessories mounted on a lathe bed.

Each part is labelled in the respective figure. The description for their functions as can be found in most related books (for example, Frocht's Photoelasticity Vol. I) is not given in this thesis.

The gear loader was originally made by Prof. H. L. Woods except for a few parts which were later made especially for this investigation.

2. The Model

The making of a model is the most important step in any photoelastic experiment. The main difficulties usually encountered are to keep the model free from initial machining stress and time edge effect.

During this investigation, repeated failures occured in this step. Columbia Resin -39 was first used to make the model, but there always revealed more or less some initial stress around the edge in cases either by hand filing or by machining with a commercial gear form cutter.

A piece of Catalin Cast Resin 61-893 (formerly known as Bakelite

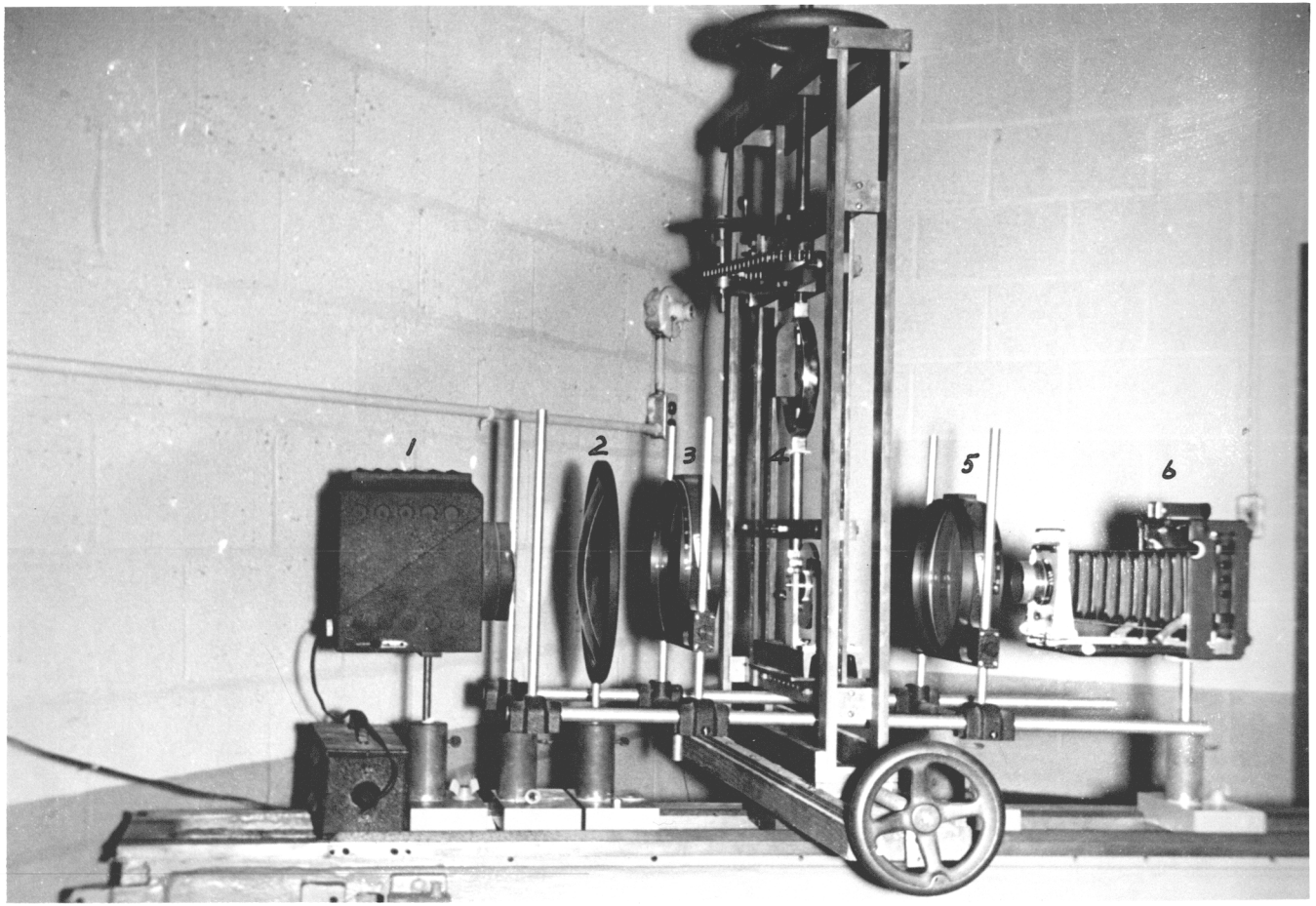

(1) Mercury Lamp with Filter (2) Lens (3) POlarizer and Quater Wave Plate

(4) Gear Model and Loading Machine (5) Analyzer and Quater Wave Plate (6) Camera

Fig. 2 - Set-up for Photographing Stress Pattern

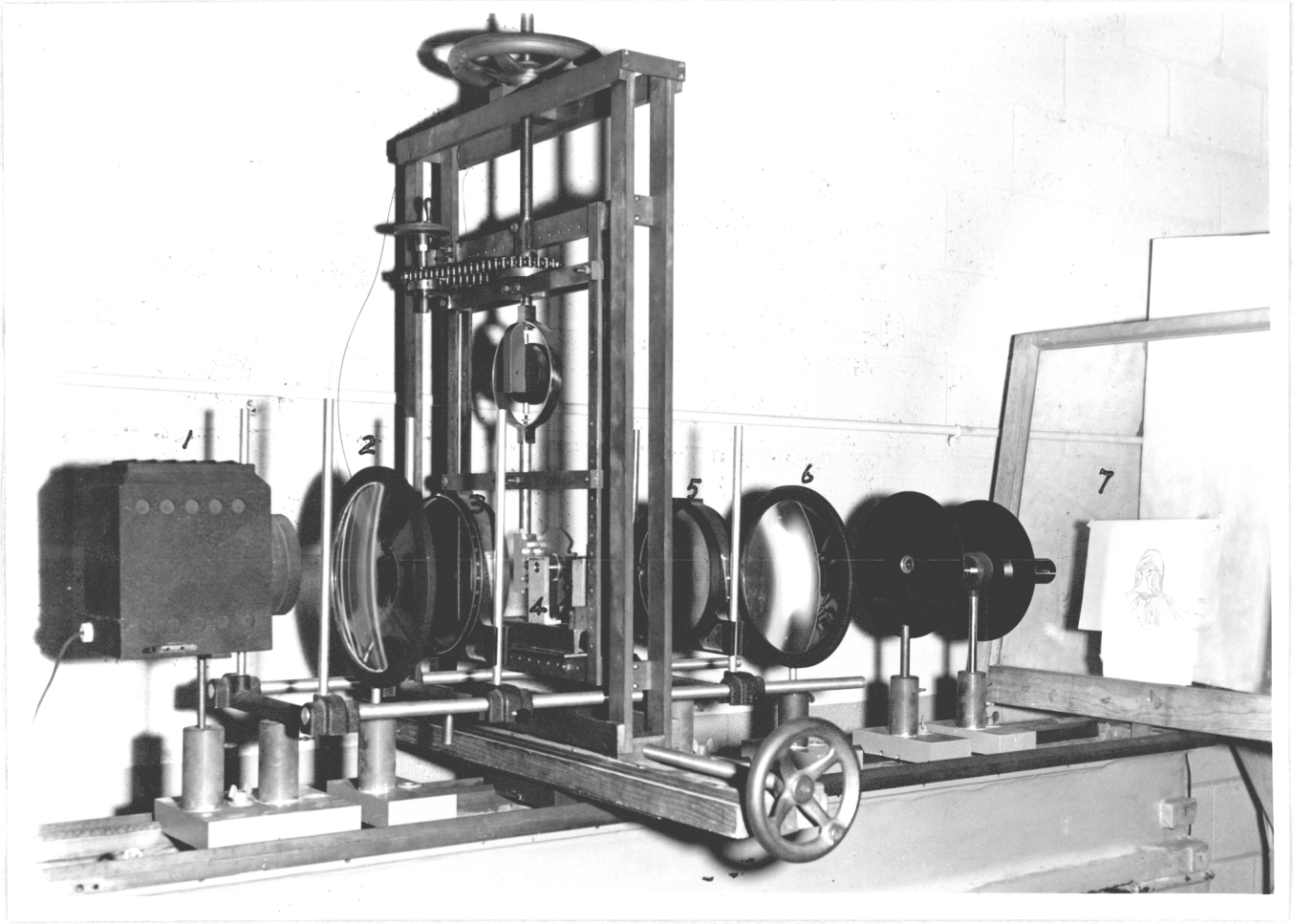

(1) White Light Source (2) Lens (3) Polarizer

(4) Model and Gear Loader (5) Analyzer (6) Lens (7) Screen

Fig. 3 - Set-up for Sketching Isoclinics

BT-61-893 was later obtained. However an initial stress still revealed down the fillets of the tooth even when carefully machined with abundant coolant. Finally a satisfactory model completely free of stress was made by filing three teeth on opposite sides as shown in Fig. 4. Its thickness is 0.279 inch.

During filing the model was clamped between two hard maple gears which served as templates. These two wood gears were originally cut by a form cutter on a milling machine.

Of course templates, if made from steel, hardened and ground after machining, will help one get a more accurate model, but this requires specialized machines which are unavailable on this campus and also requires high technique of gear making.

The above experience should not be interpreted as meaning these materials are not machinable. The machining stress depends upon several factors such as the available equipment, the cutting speed and depth, and the boundary shape of the model. Usually the more rigid and accurate the machine, the sharper the cutter, the smaller the cutting depth, the slower the cutting speed, the simpler the boundary shape, the less the machining stress will be.

According to the experience obtained during this investigation, the generation of heat is much more detrimental to Columbia Resin-39 than it is to Catalin Cast Resin 61-893.

The profile of the filed test tooth was compared with that of the machined tooth shown in Fig. 32. Both profiles were magnified under

the same setup. The small difference between them is negligible.

To diminish the time effect, the gear model was always stored in a glass dessicator as soon as it was not in use. The dessicator contained concentrated sulfuric acid as the drying agent. Practically no time effect was found during this investigation though it was sometimes left in the air for 5 or 6 hours.

D. Testing Procedures

Before the test starting, all of the components of the polariscope and accessories were properly aligned along a common axis; the light source, lens, and camera for photographing or screen for sketching were well located and focused so that a sharp-edged image appeared over the ground glass of the camera or over the screen. Clamp screws were then tightly fastened to the components in position.

The gear model was clamped between two discs so as to prevent it from any lateral twisting. The loading mechanism is shown in Fig. 4. The dial gage of the loading mechanism rendered a direct reading of the load.

The loading point was so determined that at a certain instant only one single tooth carried the full load, i.e. just after the previous tooth leaving contact and before the next tooth coming into contact (see Fig. 5). The teeth of the model and rack were oiled with a light lubricant to reduce the friction before they were brought into position.

Due to poor fitting of the loading machine, it was found that

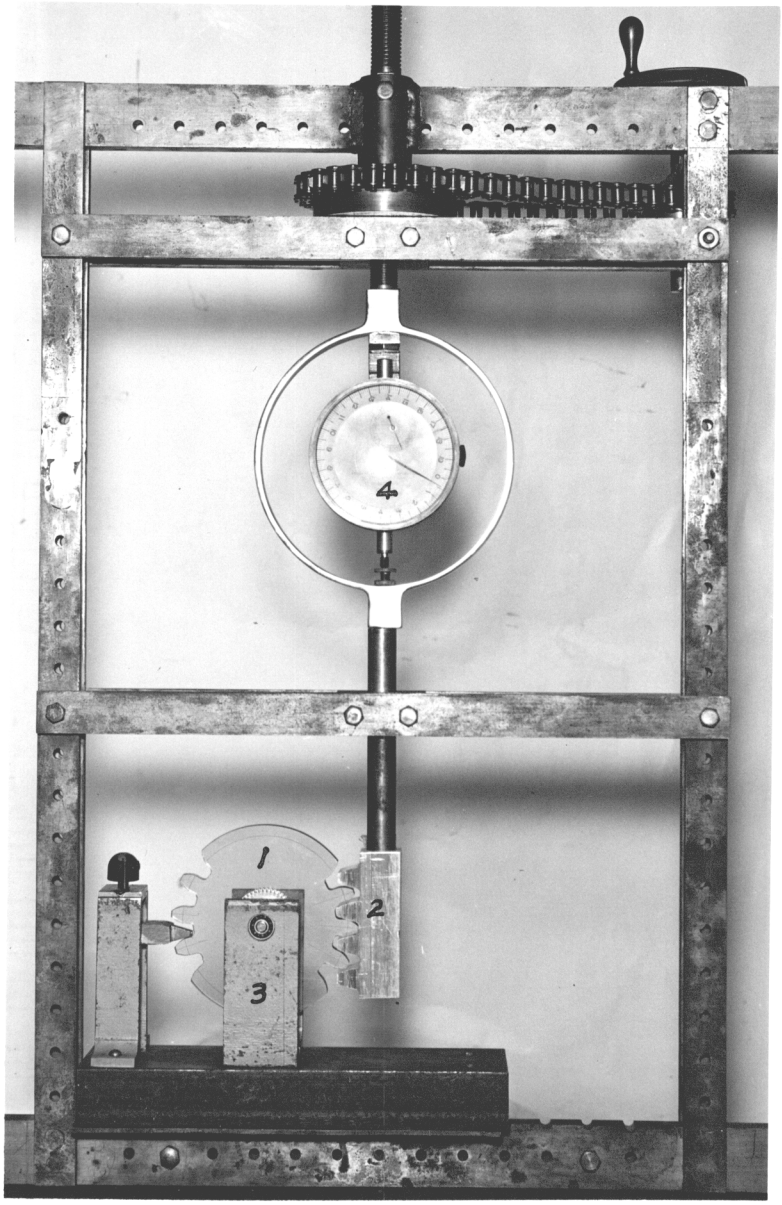

(1) Model (2) Rack

(3) Gear Loader (4) Dial Gage

Fig. 4- Loading of Model

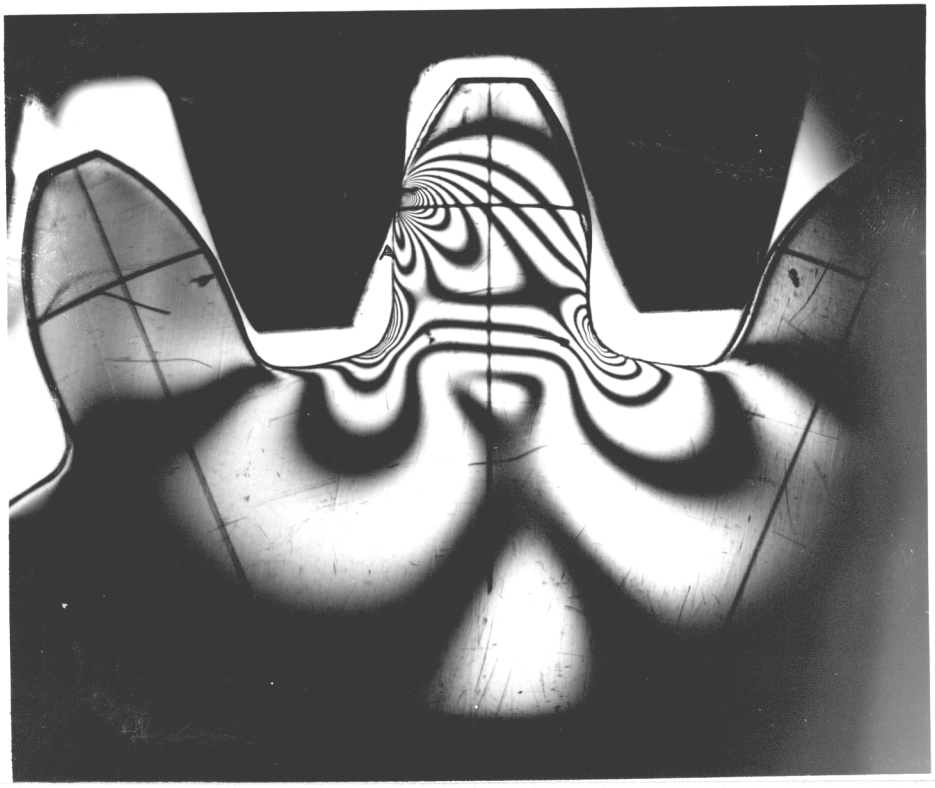

The loading point, A, was so determined that at a certain instant only one single tooth carried the full load, i.e. just before the previous tooth leaving contact.

Fig. 8 - Determination of the Loading point

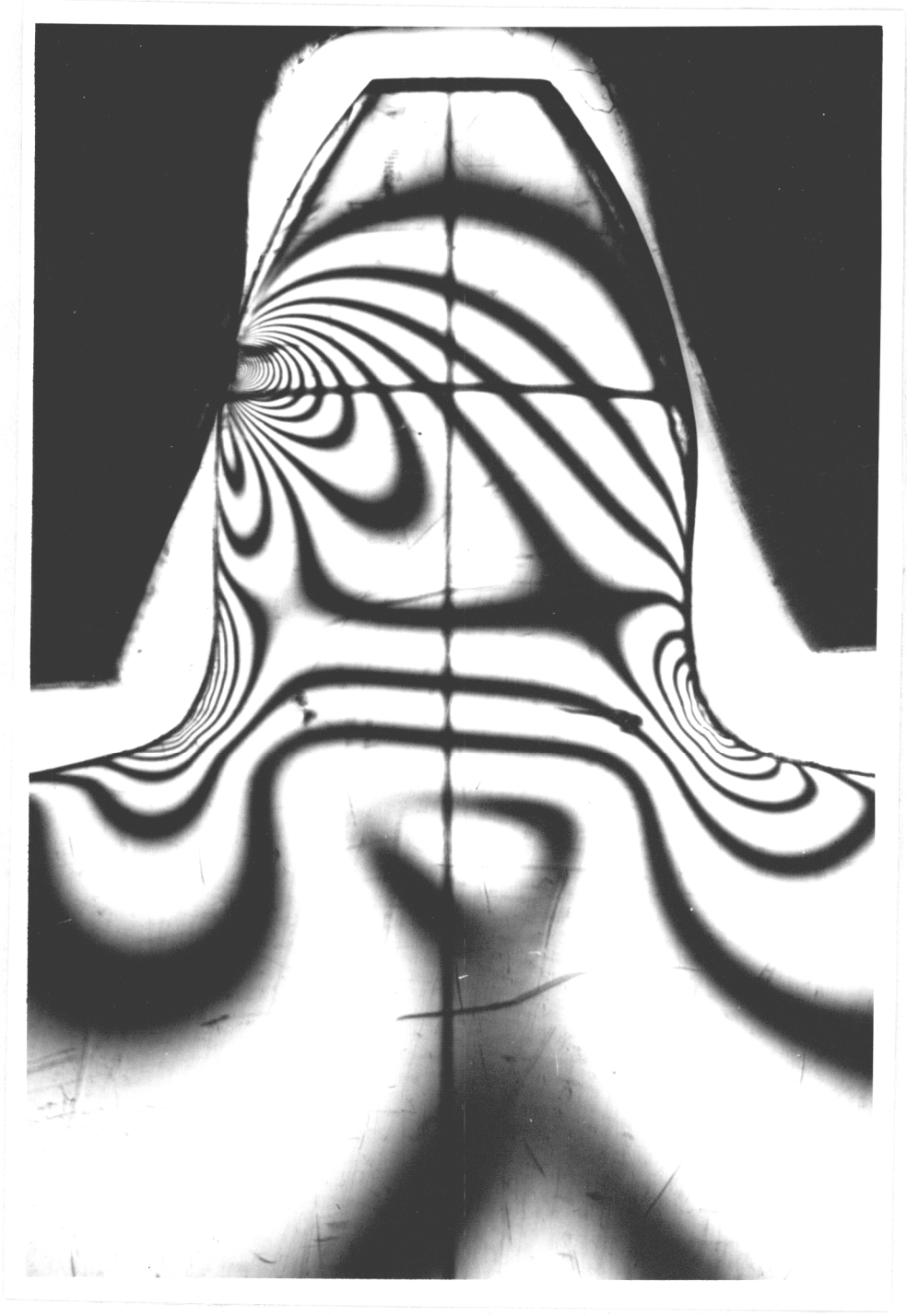

Fig. 6 - Fringe Pattern (Light Field)

Fig. 7 - Fringe Pattern (Dark Field)

when the load was being applied, the rack twisted slightly. This twisting action caused the load not to be uniformly distributed across the face of tooth and consequently some discontinuous fringes appeared on the fringe pictures. This defect however was later corrected.

Two fringe pictures were taken with a dark field and a light field respectively. First Strobolume Flash light was used, the pictures obtained appeared a little vague, but the mercury lamp light later gave better pictures as shown in Figures 6 and 7 on which the computation for this investigation is based. The film used thoroughout this investigation was the Kodak Contrast Process Ortho.. The exposure time was 1 second.

Isoclinics (see Fig.8) were directly sketched against a glass screen with quarter wave plates removed and with white light in place of mercury vapor light. The setup for this purpose is illustrated in Fig. 3.

As mentioned above, when the rack slightly twisted, part of the isoclinics was too faint to be visible. But once it was corrected, the isoclinics appeared very clear. In addition to direct sketching, isoclinics were also photographed for the purpose of further correction as shown in Figures 33 and 34. In these pictures only the curves that change with different parameters are the isoclinics.

A load of 55 lbs. as read from the dial gage was applied during photographing and sketching. Generally isoclinics are independent of load only if they appear very clear for every parameter. But in this case, due to the bending deflection of the tooth, the loading point

changes when a greater load is applied. Hence the same loading condition was maintained for both cases.

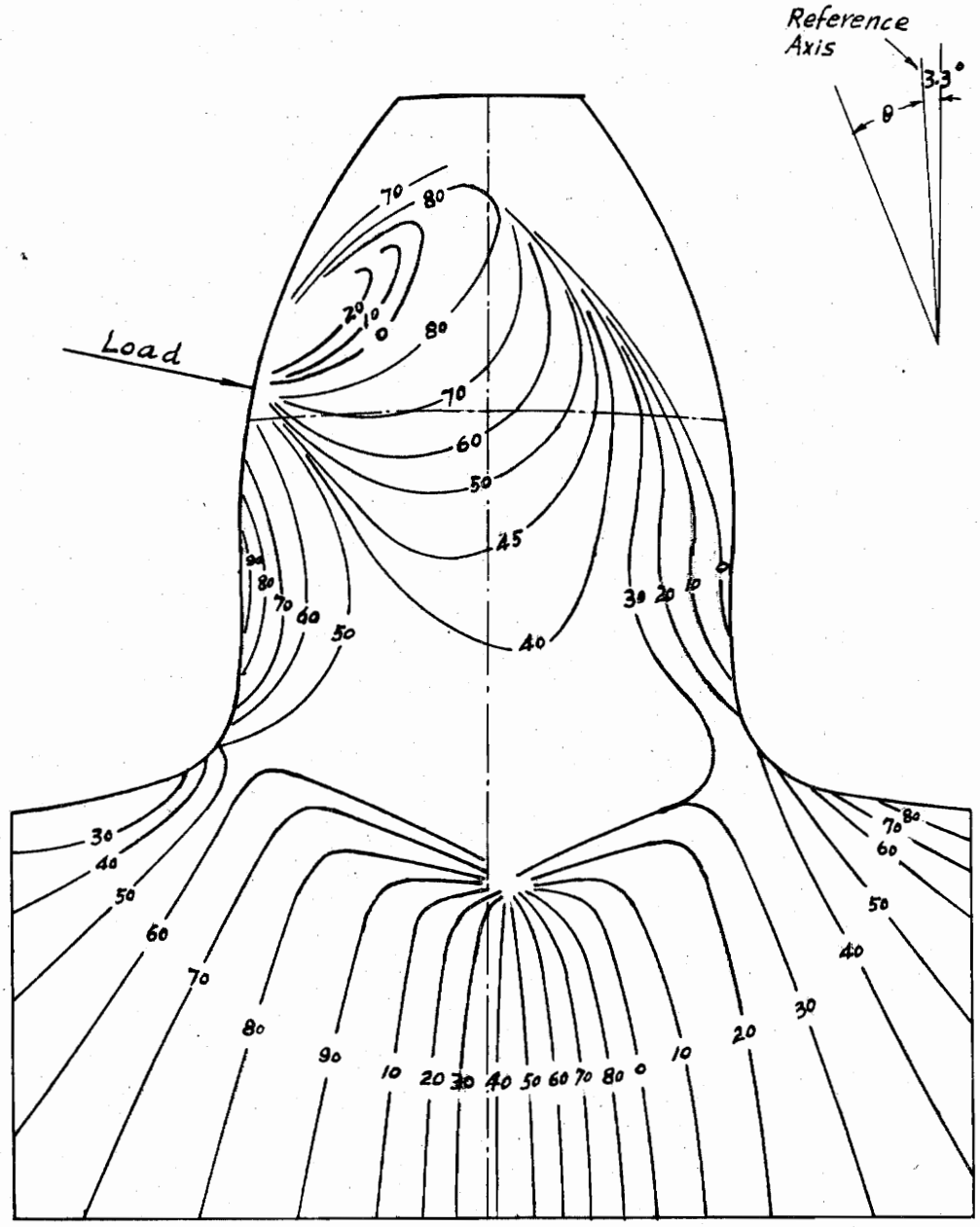

Fig. 8 - Isoclinics

VII. DISCUSSION OF RESULTS

1. Sub-surface Stresses

The numerical values of the principal stresses p and q are given in Fig. 29. These values are also presented graphically in Figures 10 and 11 from which it was learned that the principal stresses decrease very rapidly below the surface of the tooth. For instance, the values of p along the section AA (see Fig. 10) decrease from 2,925 psi (n = 9) to 975 psi (n = 3) measured 0.061 inch below the surface, a decrease of 66.7 per cent. It was also noted in Figures 10 and 11 that the (p-q) curves along the same line AA are fairly close to that of p and q. For practical purposes, the (p-q) curves may be taken as an approximation of p and q without any appreciable difference. Thus the calculation work involved may be avoided.

2. Surface Stresses

The surface stresses near the fillets of the tooth are shown graphically in Fig. 9 which indicates that the surface stresses change considerably from points near the pitch line to the fillets. This fact implies that the gear stresses do not follow Lewis' formula. In other words, this implies the existence of stress concentration.

3. Stress Concentration Factor

A factor of stress concentration was worked out by comparing the tensile stress determined photoelastically with that obtained from Lewis' formula. The point under consideration was determined graphically

according to the Lewis method as shown in Fig. 31. Thus the section AA was chosen as the critical section. The stress concentration factor was finally calculated to be 1.68.

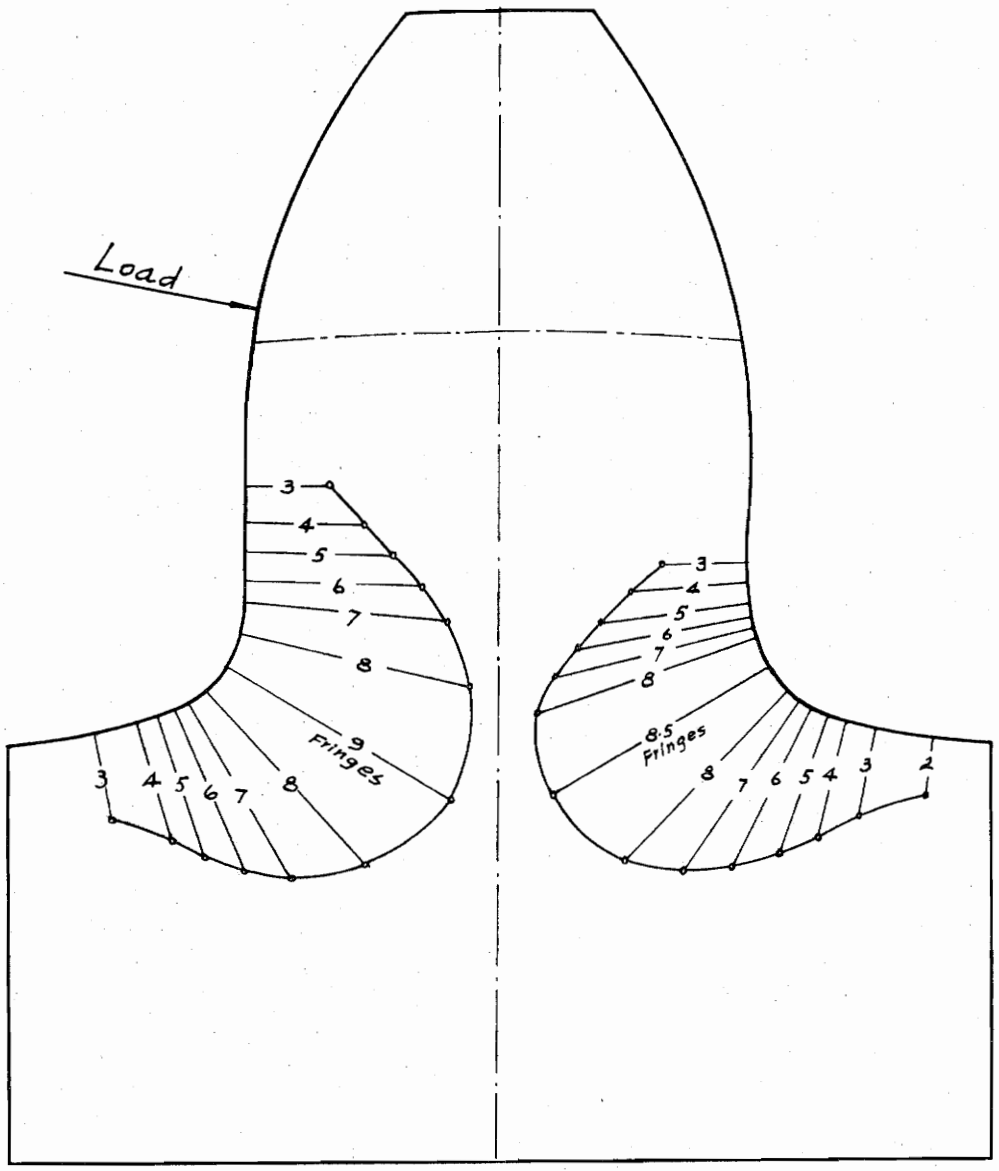

Fig. 9 - Surface Stresses

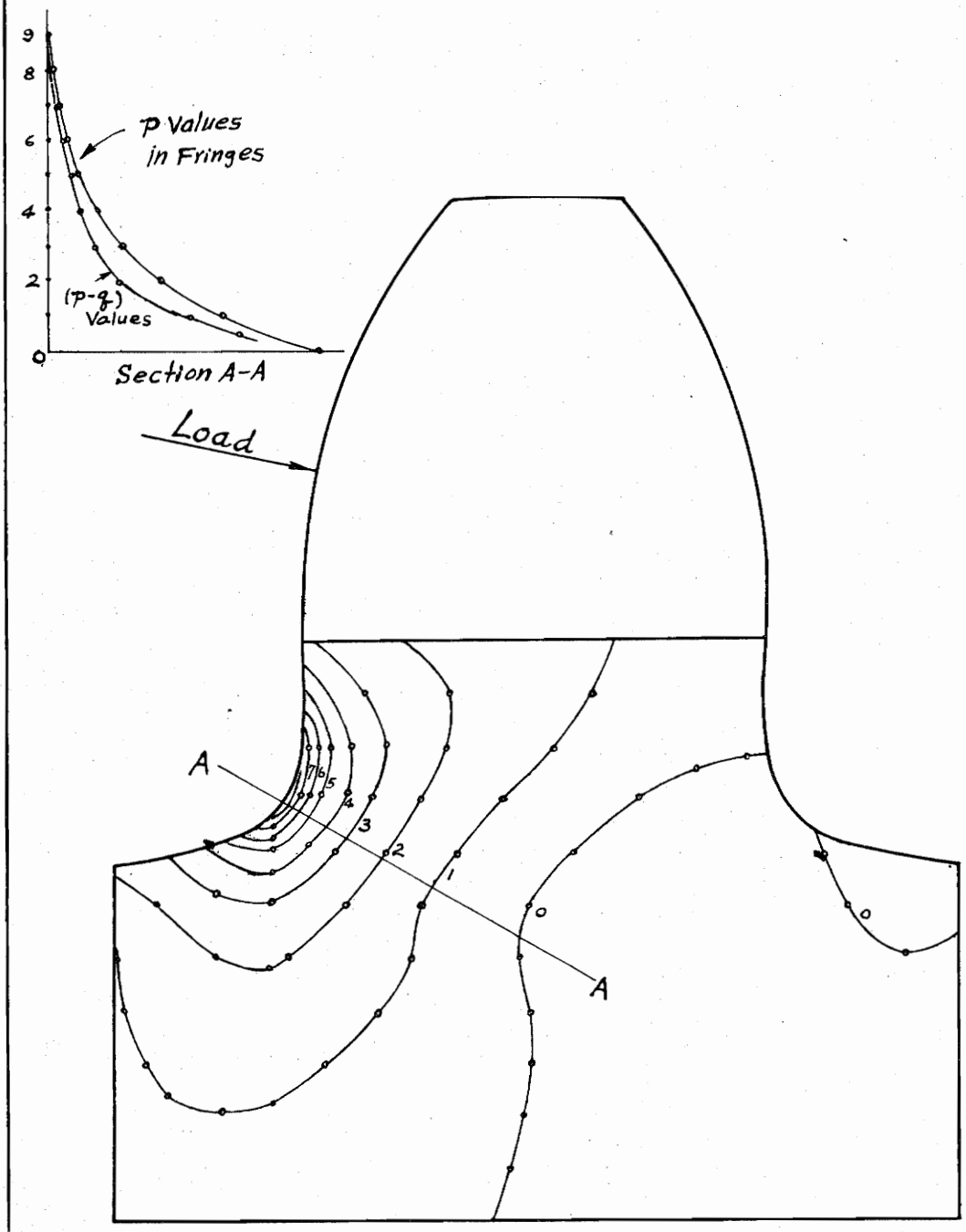

Fig. 10 - p Stress Contours

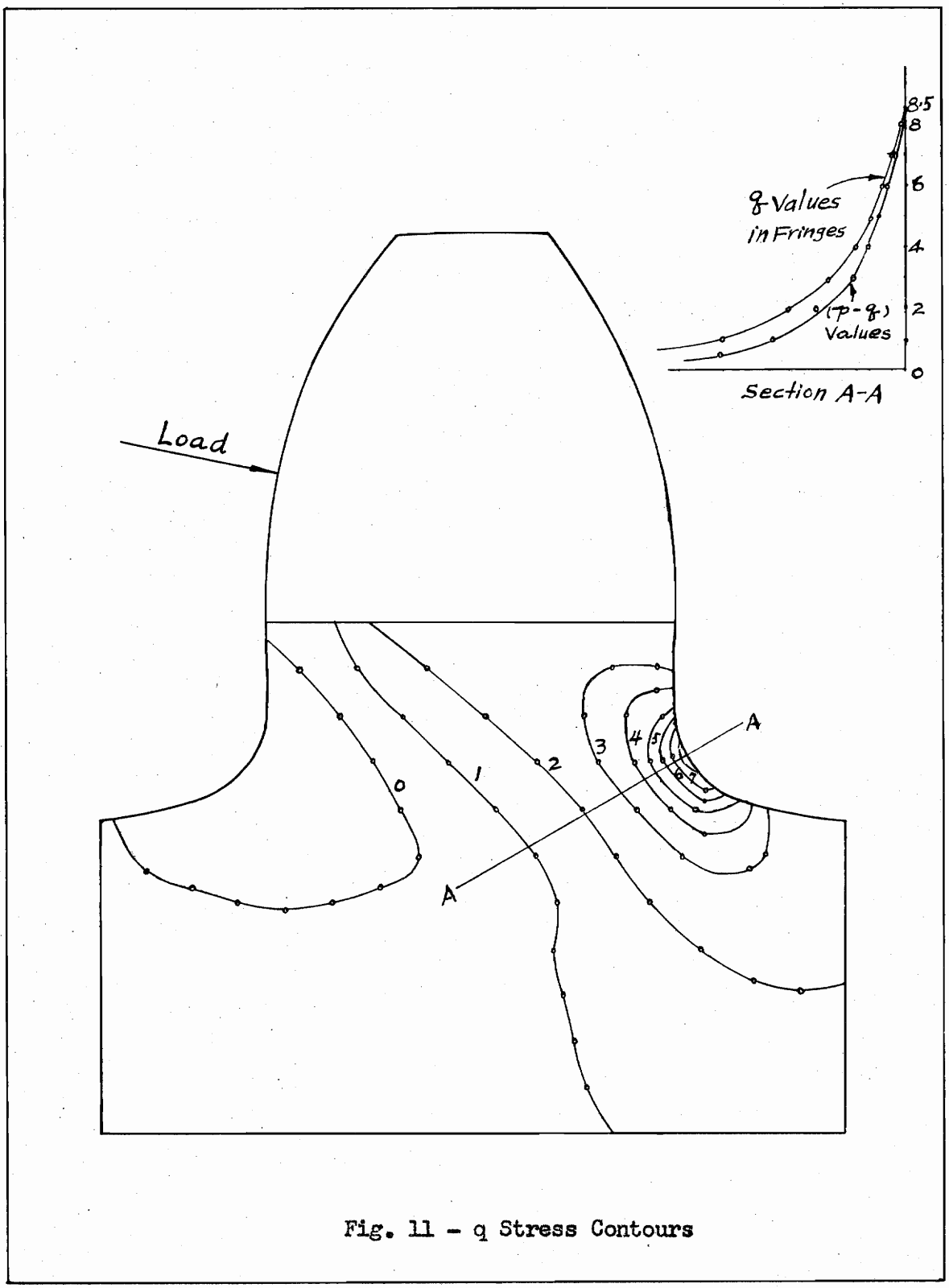

Fig. 11 - q Stress Contours

VIII. CONCLUSIONS

As pointed out in the "Discussion of Results", the sub-surface stresses in a gear tooth decrease very rapidly with its depth. This result serves as a supporting evidence to the common practice of case-hardening the gear teeth. Previously this was done according to the mechanical properties of the gear materials, but without any analytical basis.

Gear stress is a very complicated problem which includes in general the static, dynamic and fatigue stresses. Most of all, many uncertainties in service such as the impact load, acceleration load and work hardening are involved. These uncertainties make it difficult to get a general solution.

The photoelastic method is an effective one for making a static study of gear stress, but it is understood that this method can not solve the whole problem. Since if the static stresses are considered, further studies covering the notch sensitivity, friction effect, dynamic effect, and load distribution are still needed.

IX. APPENDIX

A. Sample Calculation

For the convenience of counting the fringe order at a point within the region being investigated, the stress patterns were superposed on a single drawing as shown in Fig. 12.

The first step in the sample calculation was to determine the coordinates. Those chosen for this investigation are shown in Fig. 13.

The sign of the shearing stress τ_{xy} was taken as positive if the shear diagonal passes through the first quadrant as referred to the coordinate system chosen for that particular boundary. This is shown in Figures 14 and 15.

The relative magnitude of σ_x and σ_y at a point was also determined graphically. The maximum principal stress makes an angle less than 45 degrees with greater normal stress. In the diagram appearing in Figures 16 and 17, q, τ_{xy} and the normal stress on the other two sides of the element were omitted for the sake of clearness.

The remaining step for evaluating the boundary values of $\sigma_x+\sigma_y$ = p+q follow the brief description in "Method of Approach". Figures 18 through 29 and Tables 1 through 19 inclusive show the data and results obtained.

Finally the harmonization of the (p+q) values was carried through twelve iterations until the change was less than 0.03 fringes. The initial values for an inside point may be taken arbitrarily. In this

investigation, the initial values were obtained by linear interpolation in x- and y-direction and these two values averaged.

To obtain the value of (p-q) for every grid point of intersection, curves were first plotted in Fig. 28 from which the values of (p-q) were taken to calculate the values appearing in Fig. 29.

Calibration for determining the fringe constant was made with a tension bar. This is discussed in the appendix. The calibration curve was plotted in Fig. 30. The material fringe value obtained is 91.6 lb./in./fringe.

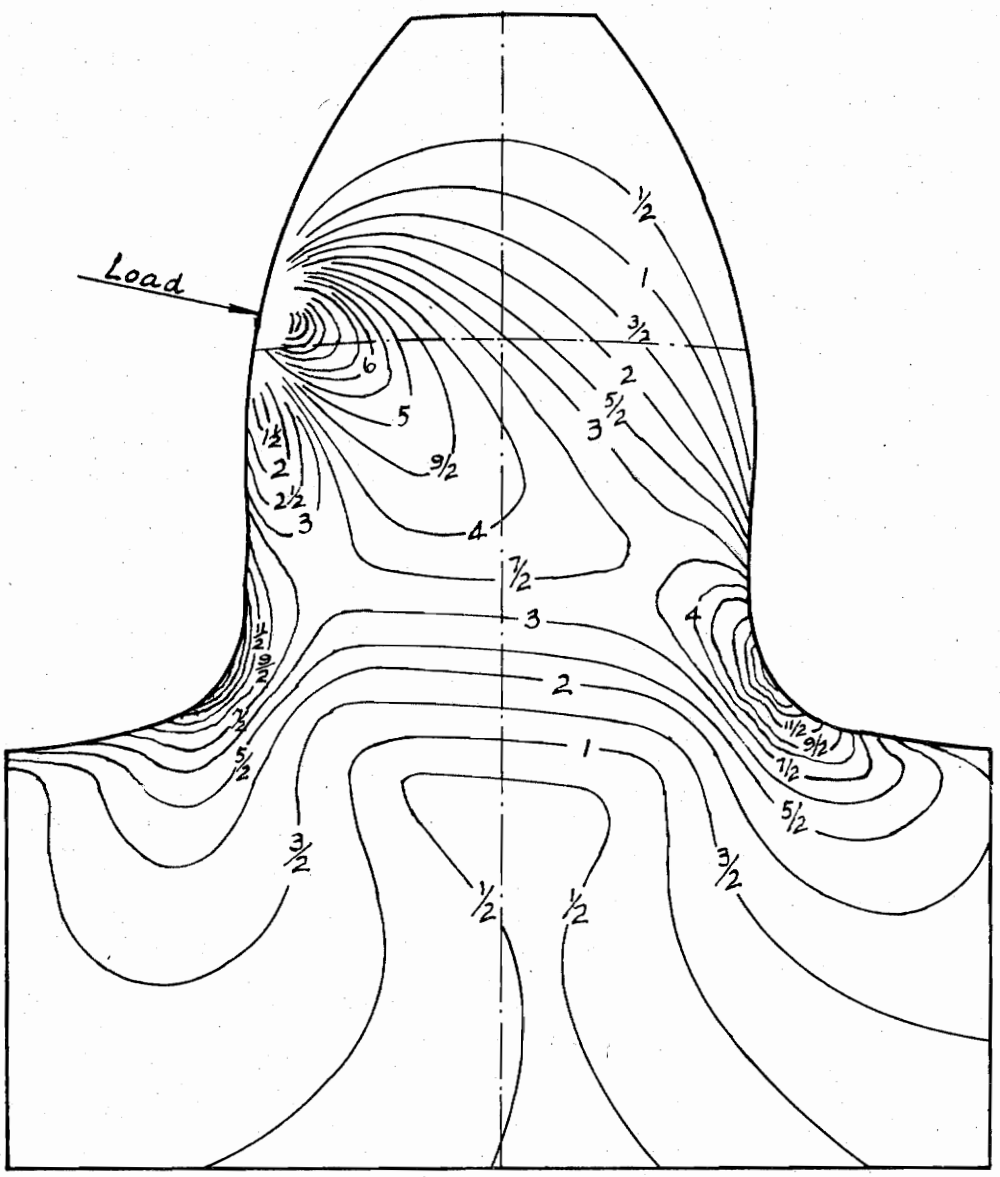

Fig. 12 - Superposed Stress Pattern

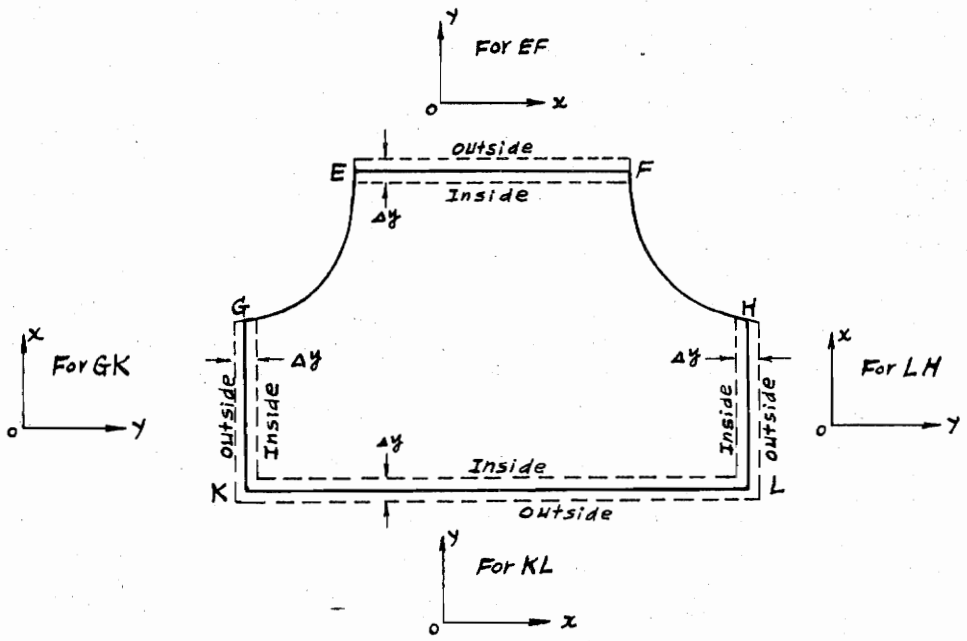

Boundary EF

In going from E to F, Δ x is + $\therefore \frac{\Delta x}{\Delta y} = +$
In going from inside to outside, Δ y is +

Boundary GK

In going from G to K, Δ x is - $\frac{\Delta x}{\Delta y} = +$
In going from inside to outside, Δ y is -

Boundary KL

In going from K to L, Δ x is + $\frac{\Delta x}{\Delta y} = -$
In going from inside to outside, Δ y is -

Boundary LH

In going from L to H, Δ x is + $\frac{\Delta x}{\Delta y} = +$
In going from inside to outside, Δ y is +

Fig. 13 - Determination of Coordinate Systems

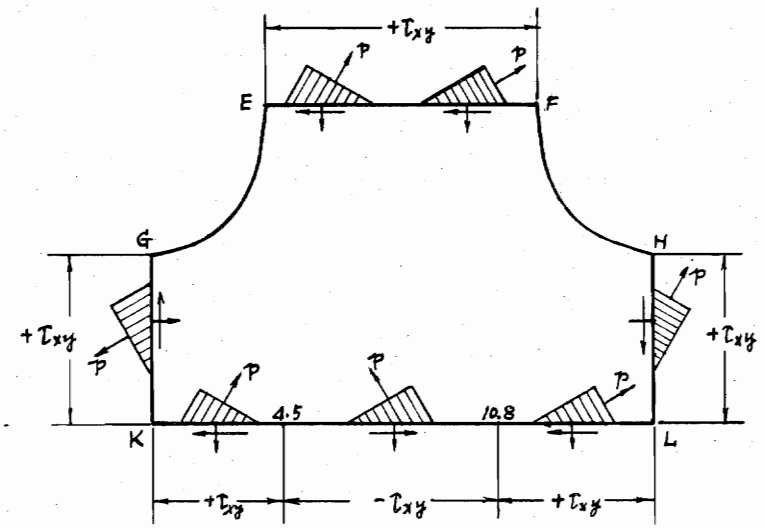

p represents maximum (algebraical) principal stress

q is not shown (not needed for the determination of the sign of τ_{xy})

Boundary EF

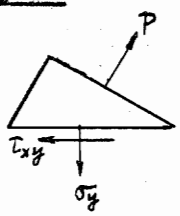

Shear Diagonal

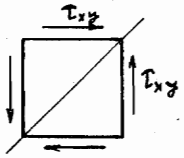

$+\tau_{xy}$

Boundary GK

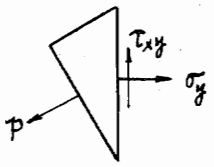

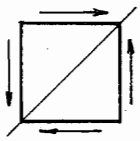

$+\tau_{xy}$

Fig. 14 - Determination of the Sign of τ_{xy}

Boundary KL, from K to 4.6

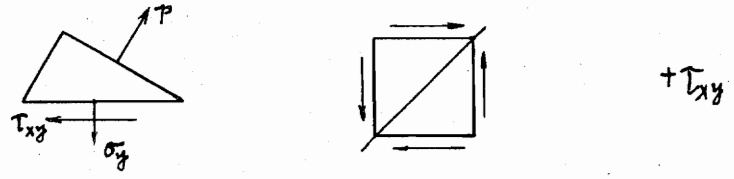

Boundary KL, from 4.6 to 10.8

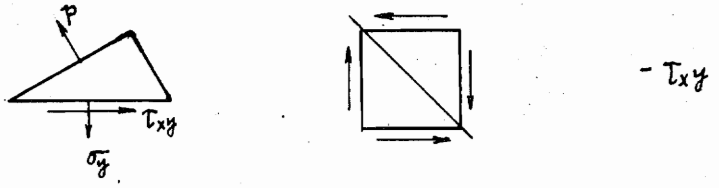

Boundary KL, 10.8 to L

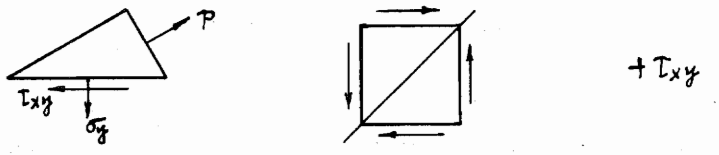

Boundary LH

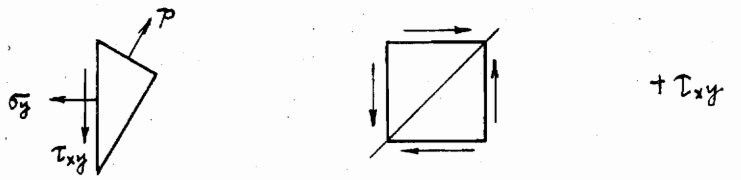

Fig. 15 - Determination of the Sign of τ_{xy} (Continued)

Boundary EF

E to 5.7

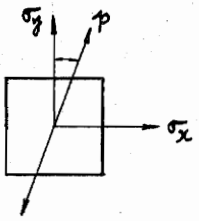

$\sigma_y > \sigma_x$

5.7 to F

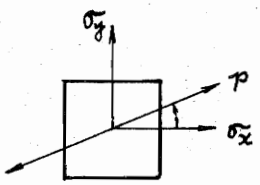

$\sigma_x > \sigma_y$

Boundary GK

G to 6.5

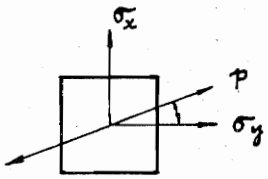

$\sigma_y > \sigma_x$

6.5 to K

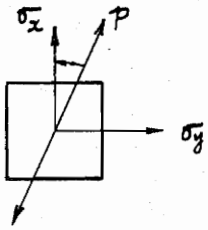

$\sigma_x > \sigma_y$

Boundary KL

K to 4.6

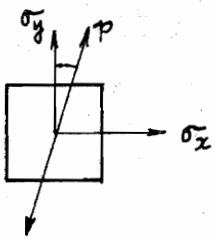

$\sigma_y > \sigma_x$

Fig. 16 - Determination of the Relative Magnitude of σ_x and σ_y

Boundary KL

4.6 to 8.4

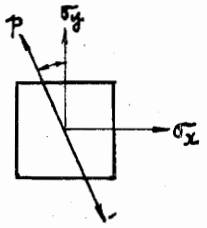

$\sigma_y > \sigma_x$

8.4 to 10.8

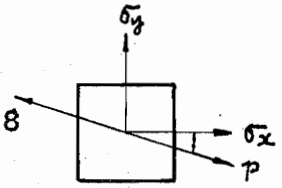

$\sigma_x > \sigma_y$

10.8 to L

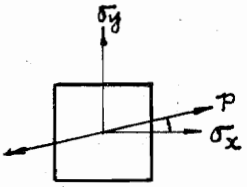

$\sigma_x > \sigma_y$

Boundary LH

L to 8.6

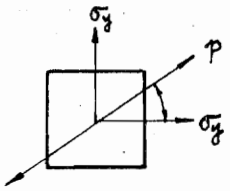

$\sigma_y > \sigma_x$

8.6 to H

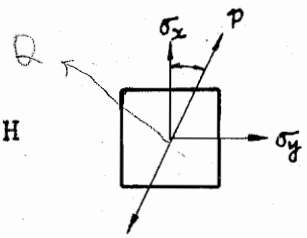

$\sigma_x > \sigma_y$

Fig. 17 - Determination of the Relative Magnitude of σ_x and σ_y (continued)

Table 1 Computation of τ_{xy}

Inside Boundary EF

Ord.	n	n/2	θ	$\theta' = \theta + 3.3$	$2\theta'$	$2\theta'$ or $180 - 2\theta'$	$\sin 2\theta'$	τ_{xy}
E	3.60	1.80	—	0.0	0.0	0.0	0.0000	0.0000
4	3.30	1.65	82.5	85.5	171.6	8.4	0.1449	0.2390
5	3.25	1.63	59.0	62.3	124.6	55.4	0.8225	1.3365
6	3.84	1.91	42.2	45.5	91.0	89.0	0.9998	1.9096
7	4.01	2.00	41.6	44.9	89.8	89.8	1.0000	2.0000
8	3.80	1.90	41.0	44.3	88.6	88.6	0.9997	1.8994
9	3.72	1.86	41.0	44.3	88.6	88.6	0.9997	1.8594
10	3.50	1.75	36.0	39.3	78.6	78.6	0.9799	1.7148
11	3.18	1.59	22.0	25.3	50.6	50.6	0.8874	1.4109
12	2.60	1.30	1.0	4.3	8.6	8.6	0.1478	0.1921
F	1.50	0.75	—	0.0	0.0	0.0	0.0000	0.0000

Boundary EF

E	3.40	1.70	—	0.0	0.0	0.0	0.0000	0.0000
4	2.50	1.25	79.0	82.3	164.6	15.4	0.2644	0.3205
5	3.10	1.55	57.5	60.8	121.6	58.4	0.8511	1.3192
6	4.02	2.01	40.0	43.3	86.6	86.6	0.9981	2.0061
7	4.18	2.09	43.5	46.8	93.6	86.4	0.9980	2.0858
8	4.05	2.02	44.0	47.3	94.6	85.4	0.9967	2.0183
9	3.76	1.88	42.0	45.3	90.6	89.4	0.9999	1.8798
10	3.35	1.67	37.0	40.3	80.6	80.6	0.9863	1.6521
11	2.82	1.41	21.0	24.3	48.6	48.6	0.7490	1.0560
12	1.95	0.97	0.0	3.3	6.6	6.6	0.1132	0.1103
F	1.40	0.70	—	0.0	0.0	0.0	0.0000	0.0000

Table 2

Computation of τ_{xy}

Outside Boundary EF

Ord.	n	n/2	θ	$\theta' = \theta + 3.3$	$2\theta'$	$2\theta'$ or $180 - 2\theta'$	$\sin 2\theta'$	τ_{xy}
E	2.75	1.38	—	0.0	0.0	0.0	0.0000	0.0000
4	2.00	1.00	77.0	80.3	160.6	19.4	0.3311	0.3311
5	3.25	1.63	55.3	58.6	117.2	62.8	0.8884	1.4436
6	4.26	2.13	42.0	45.3	90.6	89.4	0.9999	2.1298
7	4.42	2.21	46.0	49.3	98.6	81.4	0.9886	2.1848
8	4.11	2.05	45.5	48.8	97.6	82.4	0.9911	2.0367
9	3.70	1.85	43.2	46.5	93.0	87.0	0.9986	1.8474
10	3.17	1.58	38.0	41.3	82.6	82.6	0.9914	1.5713
11	2.50	1.25	19.0	22.3	44.6	44.6	0.7009	0.8759
12	1.38	0.69	0.0	3.3	6.6	6.6	0.1132	0.0781
F	0.50	0.25	—	0.0	0.0	0.0	0.0000	0.0000

Table 3

Computation of $\Delta\tau_{xy}$

Boundary EF

Ordinate	τ_{xy} (outside)	τ_{xy} (inside)	$\Delta\tau_{xy}$
E	0.0000	0.0000	0.0000
4	0.3311	0.2390	0.0921
5	1.4436	1.3365	0.1071
6	2.1298	1.9096	0.2202
7	2.1848	2.0000	0.1848
8	2.0367	1.8994	0.1373
9	1.8474	1.8594	-0.0120
10	1.5713	1.7148	-0.1435
11	0.8759	1.4109	-0.5350
12	0.0781	0.1929	-0.1148
F	0.0000	0.0000	0.0000

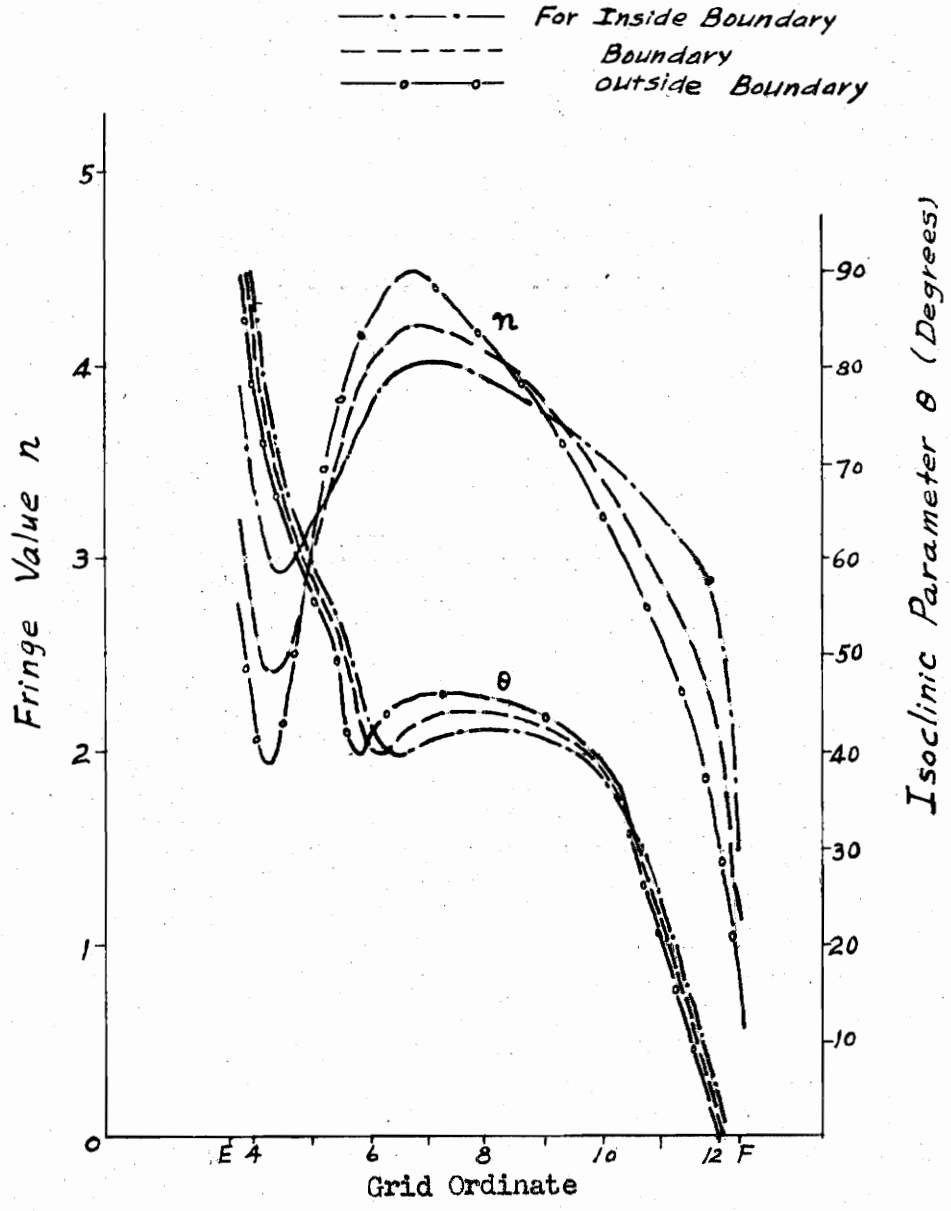

Fig. 18 - Curves of "n" and "θ"
Boundary EF

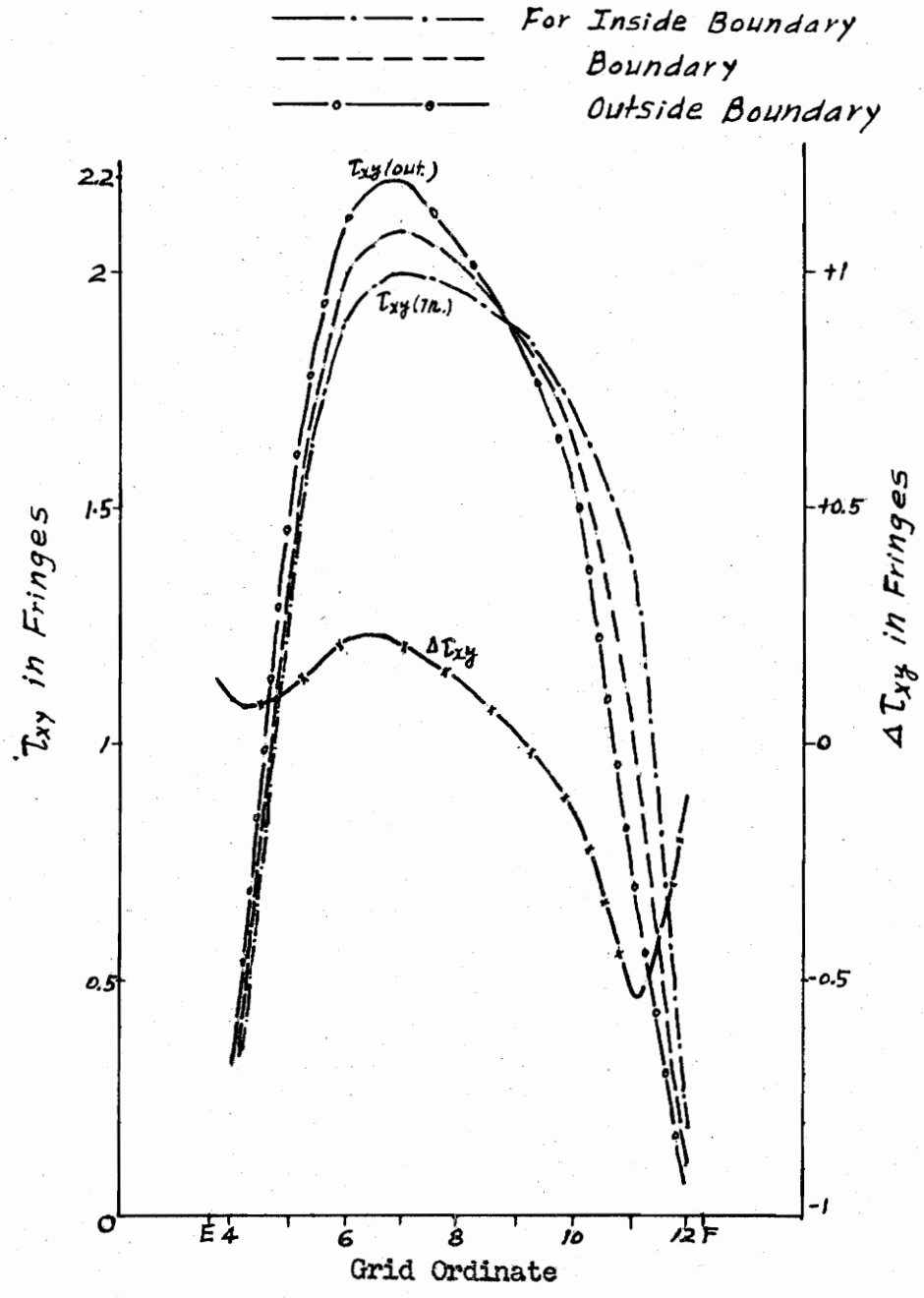

Fig. 19 - Curves of τ_{xy} and $\Delta\tau_{xy}$
Boundary EF

Point E

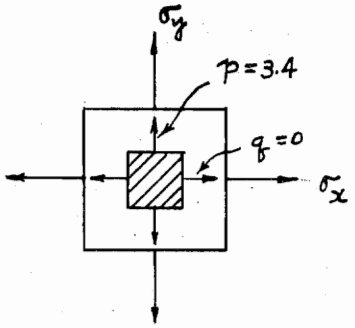

$\sigma_x = q = 0$

$\sigma_y = p = 3.4$ (Fringes)

Point F

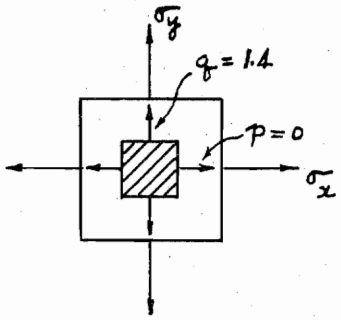

$\sigma_x = p = 0$

$\sigma_y = q = -1.4$ (Fringes)

Fig. 20 - Computation of σ_x and σ_y at Points E and F

Table 4

Computation of σ_x

Boundary EF

Ord.	$\Delta\tau_{xy}$	$\frac{\Delta x}{\Delta y}$	$\sigma_{x(n-1)}$	$\sigma_{x(n)}$
E	0.0000	—	—	0.0000
4	0.0921	0.4	0.0000	-0.0368
5	0.1071	1	-0.0368	-0.1439
6	0.2202	1	-0.1439	-0.3641
7	0.1848	1	-0.3641	-0.5489
8	0.1373	1	-0.5489	-0.6862
9	-0.0120	1	-0.6862	-0.6742
10	-0.1435	1	-0.6742	-0.5307
11	-0.5350	1	-0.5307	0.0043
12	-0.1148	1	0.0043	0.1191
F	0.0000	0.4	0.1191	0.1191

Table 5

Computation of σ_y

Boundary EF

(1) Ord.	(2) (p-q)	(3) $(p-q)^2$	(4) τ_{xy}	(5) $4\tau_{xy}^2$	(6) (3-5)	(7) $\sqrt{6}$	(8) σ_x	(9) σ_y	(10) $\sigma_y > \sigma_x$ or $\sigma_x > \sigma_y$
E	3.40	11.5600	0.0000	0.0000	11.5600	3.4000	0.0000	3.4000	$\sigma_y > \sigma_x$
4	2.50	6.2500	0.3205	0.4108	5.8392	2.4166	-0.0358	2.3798	↓
5	3.10	9.6100	1.3192	6.9608	2.6492	1.6278	-0.1439	1.4839	↓
6	4.02	16.1604	2.0061	16.0976	0.0628	0.2505	-0.3641	-0.1136	↓
7	4.18	17.4724	2.0858	17.4020	0.0704	0.2654	-0.5489	-0.8142	$\sigma_x > \sigma_y$
8	4.05	16.4025	2.0183	16.2940	0.1085	0.3286	-0.6862	-1.0148	↓
9	3.76	14.1376	1.8798	14.1344	0.0032	0.0556	-0.6742	-0.7298	↓
10	3.35	11.2225	1.6520	10.9164	0.3061	0.5531	-0.5307	-1.0838	↓
11	2.82	7.9524	1.0560	4.4604	3.4920	1.8681	0.0043	-1.8638	↓
12	1.95	3.8025	0.1103	0.0484	3.7541	1.9365	0.1191	-1.8174	↓
F	1.40	1.9600	0.0000	0.0000	1.9600	1.4000	0.1191	-1.2809	↓

Table 6

Computation of $\sigma_x + \sigma_y = p + q$

Boundary EF

Ord.	σ_x	σ_y	$\sigma_x + \sigma_y = p + q$	Corrected $p + q$
E	0.0000	3.4000	3.4000	3.40
4	-0.0358	2.3798	2.3430	2.34
5	-0.1439	1.4839	1.3400	1.30
6	-0.3641	-0.1136	-0.4777	-0.50
7	-0.5489	-0.8142	-1.3631	-1.45
8	-0.6862	-1.0148	-1.7010	-1.81
9	-0.6742	-0.7298	-1.4040	-1.55
10	-0.5307	-1.0838	-1.6145	-1.68
11	0.0043	-1.8638	-1.8593	-2.05
12	0.1191	-1.8174	-1.6983	-1.92
F	0.1191	-1.2809	-1.1618	-1.40

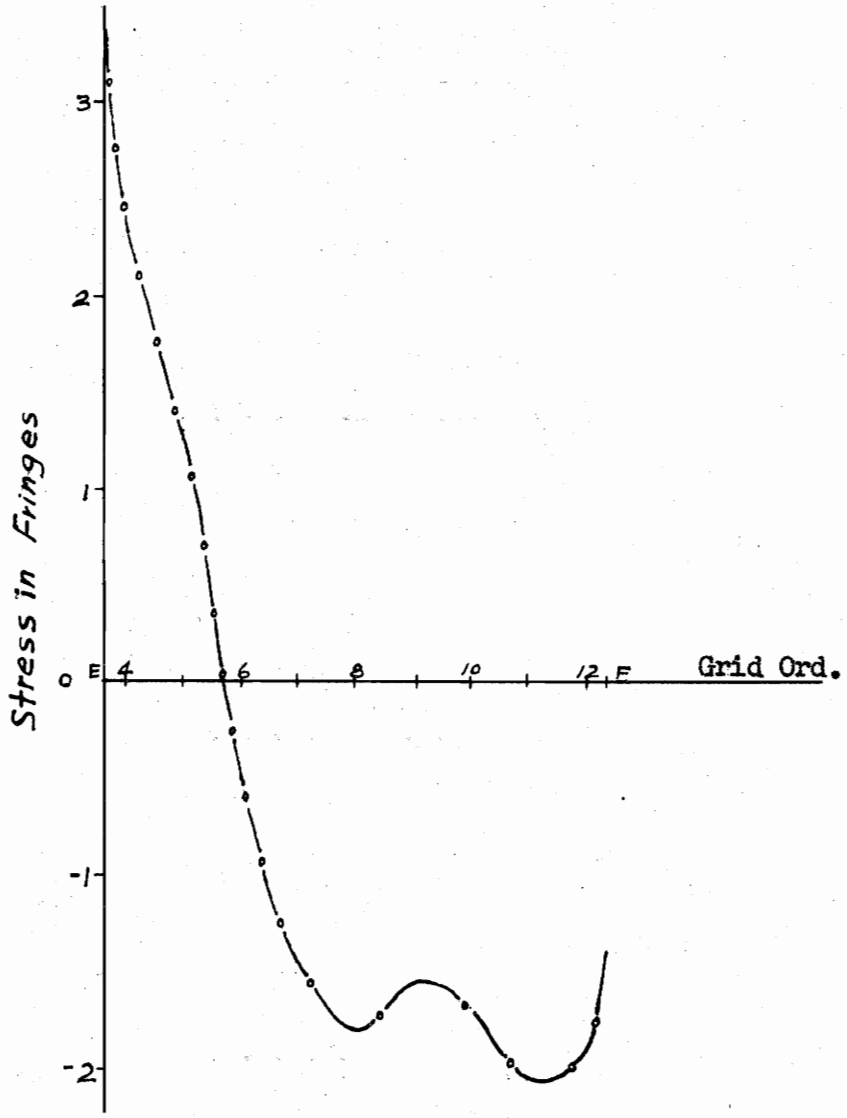

Fig. 21 - Curve of Corrected p+ q

Table 7 Computation of τ_{xy}

Inside Boundary GK

Ord.	n	n/2	θ	$\theta' = \theta + 3.3$	$2\theta'$	$2\theta'$ or $180-2\theta'$	$\sin 2\theta'$	τ_{xy}
G	(not necessary to compute)							
5	1.80	0.90	31.5	34.8	69.6	69.6	0.9367	0.8430
6	1.58	0.79	44.0	47.3	94.6	85.4	0.9969	0.7875
7	1.45	0.72	52.0	55.3	110.6	69.4	0.9356	0.6783
8	1.32	0.66	57.0	60.3	120.6	59.4	0.8601	0.5676
9	1.22	0.61	61.0	64.3	128.6	51.4	0.7808	0.4762
10	1.11	0.56	64.5	67.8	135.6	44.4	0.6988	0.3948
K	1.02	0.51	68.0	71.3	142.6	37.4	0.6065	0.3093

Outside Boundary GK

G	(not necessary to compute)							
5	1.35	0.67	28.0	31.3	63.6	63.6	0.8949	0.6040
6	1.25	0.62	39.0	42.3	84.6	84.6	0.9954	0.6221
7	1.17	0.58	47.0	50.3	100.6	79.4	0.9827	0.5748
8	1.12	0.56	52.0	55.3	110.6	69.4	0.9356	0.5239
9	1.07	0.53	56.5	59.8	119.6	60.4	0.8689	0.4648
10	1.02	0.52	60.0	63.3	126.6	53.4	0.8021	0.4090
K	1.00	0.50	63.2	66.5	133.0	47.0	0.7314	0.3657

Table 8 Computation of τ_{xy}

Boundary GK

Ord.	n	n/2	θ	$\theta' = \theta + 3.3$	$2\theta'$	$2\theta'$ or $180-2\theta'$	$\sin 2\theta'$	τ_{xy}
G	2.50	—	—	—	—	—	—	—
5	1.40	0.70	30.0	33.3	66.6	66.6	0.9171	0.6419
6	1.30	0.65	41.5	44.8	89.6	89.6	1.0000	0.6500
7	1.22	0.61	49.2	52.5	105.0	75.0	0.9659	0.5891
8	1.15	0.57	54.5	57.8	115.6	64.4	0.9013	0.5182
9	1.10	0.55	58.7	62.0	124.0	56.0	0.8290	0.4559
10	1.05	0.52	62.2	65.5	131.0	49.0	0.7547	0.3962
K	1.00	0.50	65.0	68.3	136.6	43.4	0.6841	0.3420

Boundary LH

L	1.19	0.60	37.0	40.3	80.6	80.6	0.9863	0.5917
10	1.34	0.67	40.2	43.5	87.0	87.0	0.9986	0.6700
9	1.50	0.75	43.7	47.0	94.0	86.0	0.9976	0.7482
8	1.70	0.85	48.0	51.3	102.6	77.4	0.9757	0.8293
7	1.90	0.95	52.5	55.8	111.6	68.4	0.9293	0.8828
6	2.12	1.06	59.5	62.8	125.6	54.4	0.8124	0.8611
5	2.25	1.12	72.0	75.3	150.6	29.4	0.4899	0.5511
H	1.40	0.70	80.2	83.5	167.0	13.0	0.2250	0.1587

Table 9 Computation of τ_{xy}

Inside Boundary LH

Ord.	n	n/2	θ	$\theta'=\theta+3.3$	$2\theta'$	$2\theta'$ or $180-2\theta'$	$\sin 2\theta'$	τ_{xy}
L	1.15	0.57	33.8	37.1	74.2	74.2	0.9621	0.5532
10	1.33	0.66	37.0	40.3	80.6	80.6	0.9863	0.6558
9	1.50	0.75	40.0	43.3	86.3	86.6	0.9981	0.7485
8	1.75	0.87	44.2	47.5	95.0	85.0	0.9962	0.8716
7	2.00	1.00	49.5	52.8	105.6	74.4	0.9628	0.9628
6	2.30	1.15	56.2	59.5	119.0	61.0	0.8746	1.0057
5	2.55	1.27	67.0	70.3	140.6	39.4	0.6338	0.8080
H	1.60	0.80	83.7	87.0	164.0	16.0	0.2756	0.2204

Outside Boundary LH

L	1.24	0.62	40.0	43.3	86.6	86.6	0.9981	0.6188
10	1.36	0.68	43.0	46.3	92.6	87.4	0.9989	0.6792
9	1.50	0.75	46.0	49.3	98.6	81.4	0.9886	0.7414
8	1.66	0.83	50.2	53.5	107.0	73.0	0.9563	0.7937
7	1.82	0.91	55.0	58.3	116.6	63.4	0.8936	0.8131
6	2.00	1.00	62.6	65.9	131.8	48.2	0.7451	0.7451
5	2.05	1.02	76.0	79.3	158.6	21.4	0.3638	0.3728
H	1.35	0.67	—	86.0	172.0	8.0	0.1392	0.0940

Table 10 Computation of $\Delta\tau_{xy}$

Boundary GK

Ord.	τ_{xy} (outside)	τ_{xy} (inside)	$\Delta\tau_{xy}$
G	(not computated)		
5	0.6040	0.8430	-0.2390
6	0.6221	0.7875	-0.1654
7	0.5748	0.6783	-0.0935
8	0.5239	0.5676	-0.0437
9	0.4648	0.4762	-0.0114
10	0.4090	0.3948	0.0142
K	0.3657	0.3093	0.0564

Boundary LH

L	0.6188	0.5532	0.0656
10	0.6792	0.6558	0.0234
9	0.7414	0.7485	-0.0071
8	0.7937	0.8716	-0.0879
7	0.8131	0.9628	-0.1497
6	0.7451	1.0057	-0.2606
5	0.3728	0.8080	-0.4352
H	0.0940	0.2204	-0.1264

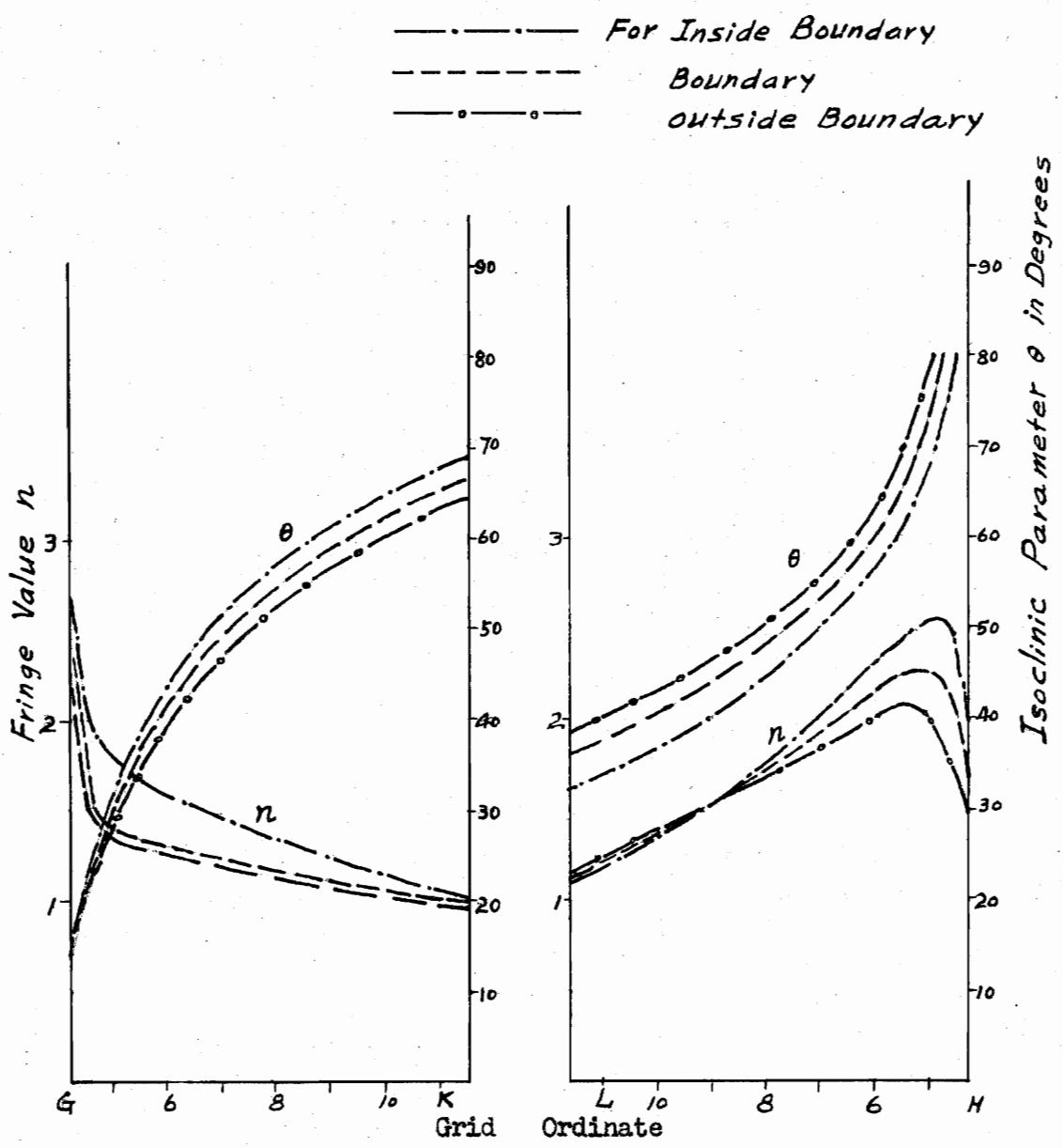

Fig. 22 - Curves of "n" and "θ"
Boundaries GK, LH

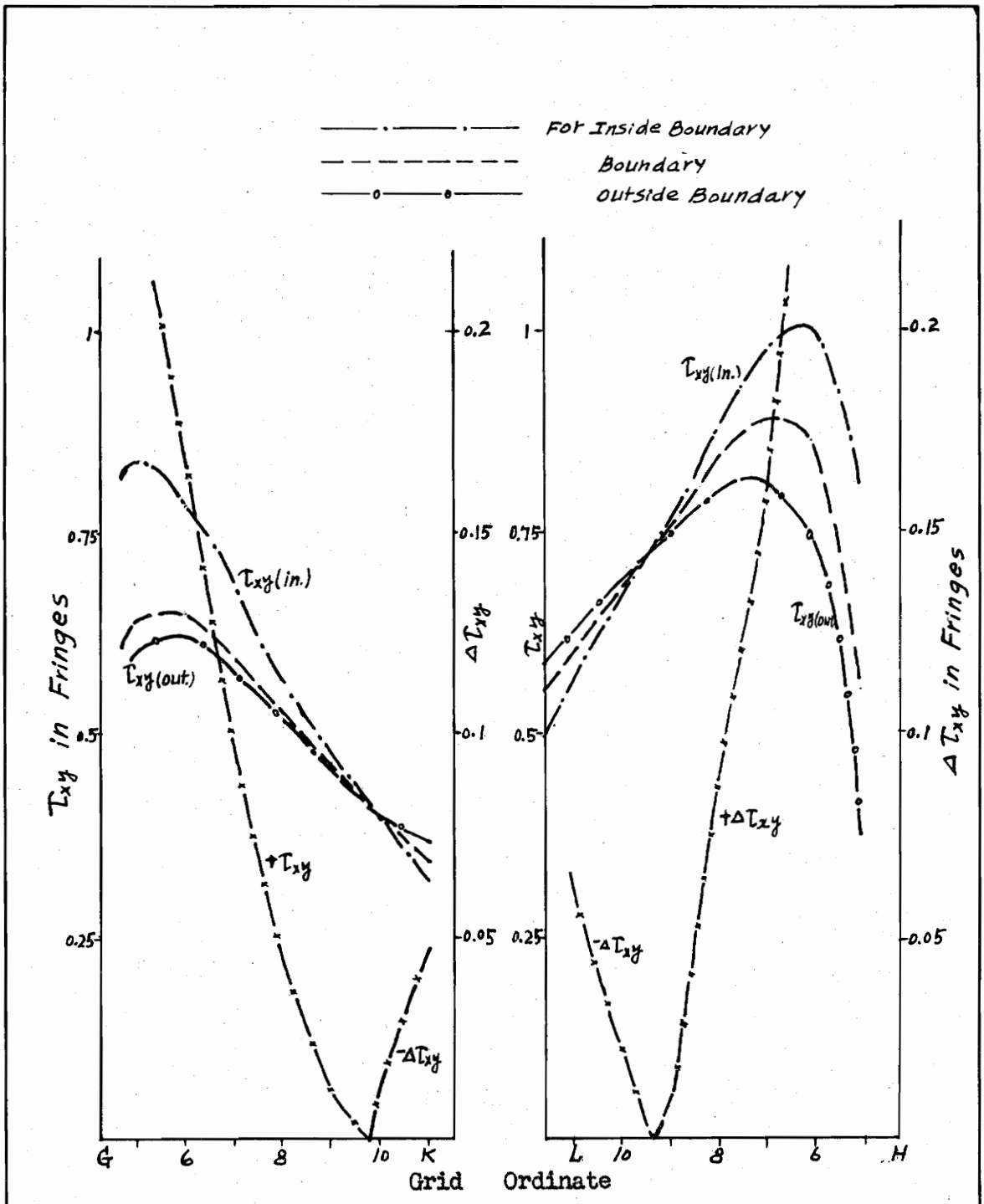

Fig. 23 - Curves of τ_{xy} and $\Delta\tau_{xy}$
Boundaries GK, LH

Point G

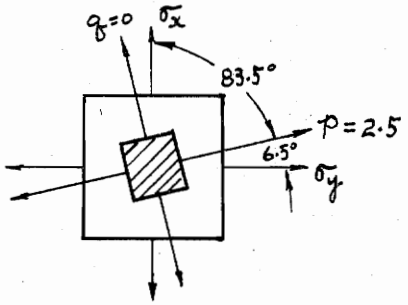

$$\sigma_x = \frac{p}{2} + \frac{p}{2}\cos(167^\circ)$$

$$= 0.0320 \text{ (Fringes)}$$

$$\sigma_y = \frac{p}{2} + \frac{p}{2}\cos(-13^\circ)$$

$$= 2.4680 \text{ (Fringes)}$$

Point H

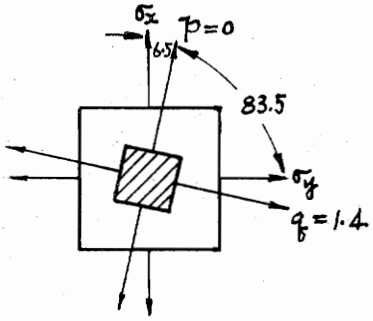

$$\sigma_x = \frac{q}{2} - \frac{q}{2}\cos(13^\circ)$$

$$= -0.0179 \text{ (Fringes)}$$

$$\sigma_y = \frac{q}{2} - \frac{q}{2}\cos(-167^\circ)$$

$$= -1.328 \text{ (Fringes)}$$

Fig. 24 - Computation of σ_x and σ_y at Points G and H

Table 11 Computation of σ_x

Boundary GK

Ord.	$\Delta\tau_{xy}$	$\frac{\Delta x}{\Delta y}$	$\sigma_{x(n-1)}$	$\sigma_{x(n)}$
G	—	—	—	0.0320
5	-0.2390	0.83	0.0320	0.2300
6	-0.1650	1	0.2300	0.3950
7	-0.0935	1	0.3950	0.4885
8	-0.0437	1	0.4885	0.5322
9	-0.0114	1	0.5322	0.5436
10	0.0142	1	0.5436	0.5294
K	0.0564	1	0.5294	0.4730

Boundary LH

L	—	—	—	-0.9396
10	0.0234	1	-0.9396	-0.9630
9	-0.0071	1	-0.9630	-0.9559
8	-0.0879	1	-0.9559	-0.8680
7	-0.1497	1	-0.8680	-0.6563
6	-0.2606	1	-0.6563	-0.3957
5	-0.4352	1	-0.3957	0.0395
H	-0.1264	0.83	0.0395	0.1444

Table 12 Computation of σ_y

Boundary GK

(1) Ord.	(2) (p-q)	(3) $(p-q)^2$	(4) τ_{xy}	(5) $4\tau_{xy}^2$	(6) (3-5)	(7) $\sqrt{6}$	(8) σ_x	(9) σ_y	(10) $\sigma_x > \sigma_y$ or $\sigma_y > \sigma_x$
G	—	—	—	—	—	—	0.0320	2.4680	$\sigma_y > \sigma_x$
5	1.40	1.9600	0.6419	1.6480	0.3120	0.5585	0.2300	0.7885	↓
6	1.30	1.6900	0.6500	1.6900	0.0000	0.0000	0.3950	0.3950	
7	1.22	1.4884	0.5891	1.3880	0.1004	0.3162	0.4885	0.1723	$\sigma_x > \sigma_y$
8	1.15	1.3225	0.5182	1.0740	0.2480	0.5000	0.5322	0.0322	
9	1.10	1.2100	0.4559	0.8312	0.3788	0.6148	0.5436	-0.0712	
10	1.05	1.1025	0.3962	0.6276	0.4749	0.6892	0.5294	-0.1598	
K	1.00	1.0000	0.3420	0.4676	0.5324	0.7293	0.4730	-0.2563	

Boundary LH

L	—	—	—	—	—	—	-0.9396	-0.7424	$\sigma_y > \sigma_x$
10	1.34	1.7956	0.6700	1.7956	0.0000	0.0000	-0.9630	-0.9630	↓
9	1.50	2.2500	0.7482	2.2392	0.0120	0.1095	-0.9559	-0.8464	
8	1.70	2.8900	0.8293	2.7508	0.1412	0.3755	-0.8680	-1.2435	$\sigma_x > \sigma_y$
7	1.90	3.6100	0.8828	3.1172	0.4216	0.6495	-0.6563	-1.3058	
6	2.12	4.4944	0.8611	2.9656	1.5288	1.2368	-0.3957	-1.6325	
5	2.25	5.0625	0.5511	1.2148	3.8477	1.9610	0.0395	-1.9215	
H	1.40	1.9600	0.1587	0.1012	2.1488	1.4663	0.1444	-1.3219	

Table 13 Computation of τ_{xy}

Inside Boundary KL

Ord.	n	n/2	θ	$\theta'=\theta+3.3$	$2\theta'$	$2\theta'$ or $180-2\theta'$	$\sin 2\theta'$	τ_{xy}
K	1.12	0.56	63.5	66.8	133.6	46.4	0.7234	0.4051
1	1.16	0.58	68.5	71.8	143.6	36.4	0.5929	0.3436
2	1.20	0.60	73.7	77.0	154.0	26.0	0.4384	0.2630
3	1.10	0.55	79.0	82.3	164.6	15.4	0.2644	0.1454
4	1.06	0.53	85.0	88.3	176.6	3.4	0.0581	0.0307
5	0.98	0.49	1.2	4.5	9.0	9.0	0.1564	-0.0766
6	0.82	0.41	10.0	13.3	26.6	26.6	0.4462	-0.1829
7	0.70	0.35	20.5	23.8	47.6	47.6	0.7373	-0.2580
8	0.55	0.27	37.0	40.3	80.6	80.6	0.9863	-0.2712
9	0.40	0.20	54.5	57.8	115.6	64.4	0.9013	-0.1802
10	0.50	0.25	75.5	78.8	157.6	22.4	0.3800	-0.0950
11	0.66	0.33	2.0	5.3	10.6	10.6	0.1822	0.0601
12	0.81	0.40	12.5	15.8	31.6	31.6	0.5225	0.2116
13	0.97	0.48	20.5	23.8	47.6	47.6	0.7373	0.3575
14	1.10	0.55	27.0	30.3	60.6	60.6	0.8704	0.4787
15	1.20	0.60	33.0	36.3	72.6	72.6	0.9537	0.5722
L	1.24	0.62	38.2	41.5	83.0	83.0	0.9925	0.6153

Table 14 Computation of τ_{xy}

Boundary KL

Ord.	n	n/2	θ	$\theta' = \theta + 3.3$	$2\theta'$	$2\theta'$ or $180 - 2\theta'$	$\sin 2\theta'$	τ_{xy}
K	1.10	0.55	65.0	68.3	136.6	43.4	0.6862	0.3774
1	1.12	0.56	70.0	73.3	146.6	33.4	0.5494	0.3077
2	1.13	0.56	75.0	78.3	156.6	23.4	0.3961	0.2237
3	1.07	0.53	80.0	83.3	166.6	13.4	0.2306	0.1233
4	0.98	0.49	86.0	89.3	178.6	1.4	0.0233	0.0114
5	0.86	0.43	1.5	4.8	9.6	9.6	0.1650	-0.0709
6	0.75	0.37	11.0	14.3	28.6	28.6	0.4772	-0.1789
7	0.61	0.30	22.0	25.3	50.6	50.6	0.7716	-0.2353
8	0.50	0.25	38.0	41.3	82.6	82.6	0.9911	-0.2477
9	0.36	0.18	52.5	55.8	111.6	68.4	0.9293	-0.1672
10	0.41	0.20	72.5	75.8	151.6	28.4	0.4746	-0.0972
11	0.60	0.30	1.0	4.3	8.6	8.6	0.1478	0.0443
12	0.75	0.37	11.6	14.9	29.8	29.8	0.4950	0.1732
13	0.88	0.44	20.0	23.3	46.6	46.6	0.7254	0.3191
14	1.00	0.50	26.4	29.7	59.4	59.4	0.8601	0.4300
15	1.11	0.55	32.0	35.3	70.6	70.6	0.9426	0.5231
L	1.19	0.59	37.0	40.3	80.6	80.6	0.9863	0.5868

Table 15 Computation of τ_{xy}

Outside Boundary KL

Ord.	n	n/2	θ	$\theta' = \theta + 3.3$	$2\theta'$	$2\theta'$ or $180 - 2\theta'$	$\sin 2\theta'$	τ_{xy}
K	1.05	0.52	66.2	69.5	139.0	41.0	0.6561	0.3444
1	1.06	0.53	71.0	74.3	148.6	31.4	0.5200	0.2756
2	1.05	0.52	76.0	79.3	158.6	21.4	0.3638	0.1909
3	1.01	0.50	81.0	84.3	168.6	11.4	0.1965	0.0992
4	0.91	0.45	87.0	90.3	180.6	0.6	0.0087	0.0039
5	0.78	0.39	2.0	5.6	11.2	11.2	0.1937	-0.0755
6	0.67	0.33	11.5	14.8	29.6	29.6	0.5075	-0.1710
7	0.51	0.25	24.0	27.3	54.6	54.6	0.8141	-0.2075
8	0.44	0.22	39.0	42.3	84.6	84.6	0.9954	-0.2189
9	0.30	0.15	51.0	54.3	108.6	71.4	0.9474	-0.1421
10	0.36	0.18	71.0	74.3	148.6	31.4	0.5200	-0.0936
11	0.52	0.26	0.0	333	6.6	6.6	0.1132	0.0294
12	0.66	0.33	11.0	14.3	28.6	28.6	0.4772	0.1574
13	0.70	0.35	19.0	22.3	44.6	44.6	0.7009	0.2453
14	0.92	0.47	25.5	28.8	57.6	57.6	0.8434	0.3879
15	1.05	0.52	31.0	34.3	68.6	68.6	0.9304	0.4884
L	1.12	0.56	36.0	39.3	78.6	78.6	0.9799	0.5487

Table 16 Computation of $\Delta\tau_{xy}$

Boundary KL

Ord.	τ_{xy} (outside)	τ_{xy} (inside)	$\Delta\tau_{xy}$
K	0.3444	0.4051	-0.0607
1	0.2756	0.3436	-0.0680
2	0.1909	0.2630	-0.0721
3	0.0992	0.1454	-0.0462
4	0.0039	0.0307	-0.0268
5	-0.0755	-0.0766	0.0011
6	-0.1810	-0.1829	0.0119
7	-0.2075	-0.2580	0.0505
8	-0.2189	-0.2712	0.0523
9	-0.1421	-0.1802	0.0381
10	-0.0936	-0.0950	0.0014
11	0.0294	0.0601	-0.0307
12	0.1574	0.2116	-0.0542
13	0.2453	0.3575	-0.1122
14	0.3879	0.4787	-0.0908
15	0.4884	0.5722	-0.0838
L	0.5487	0.6153	-0.0666

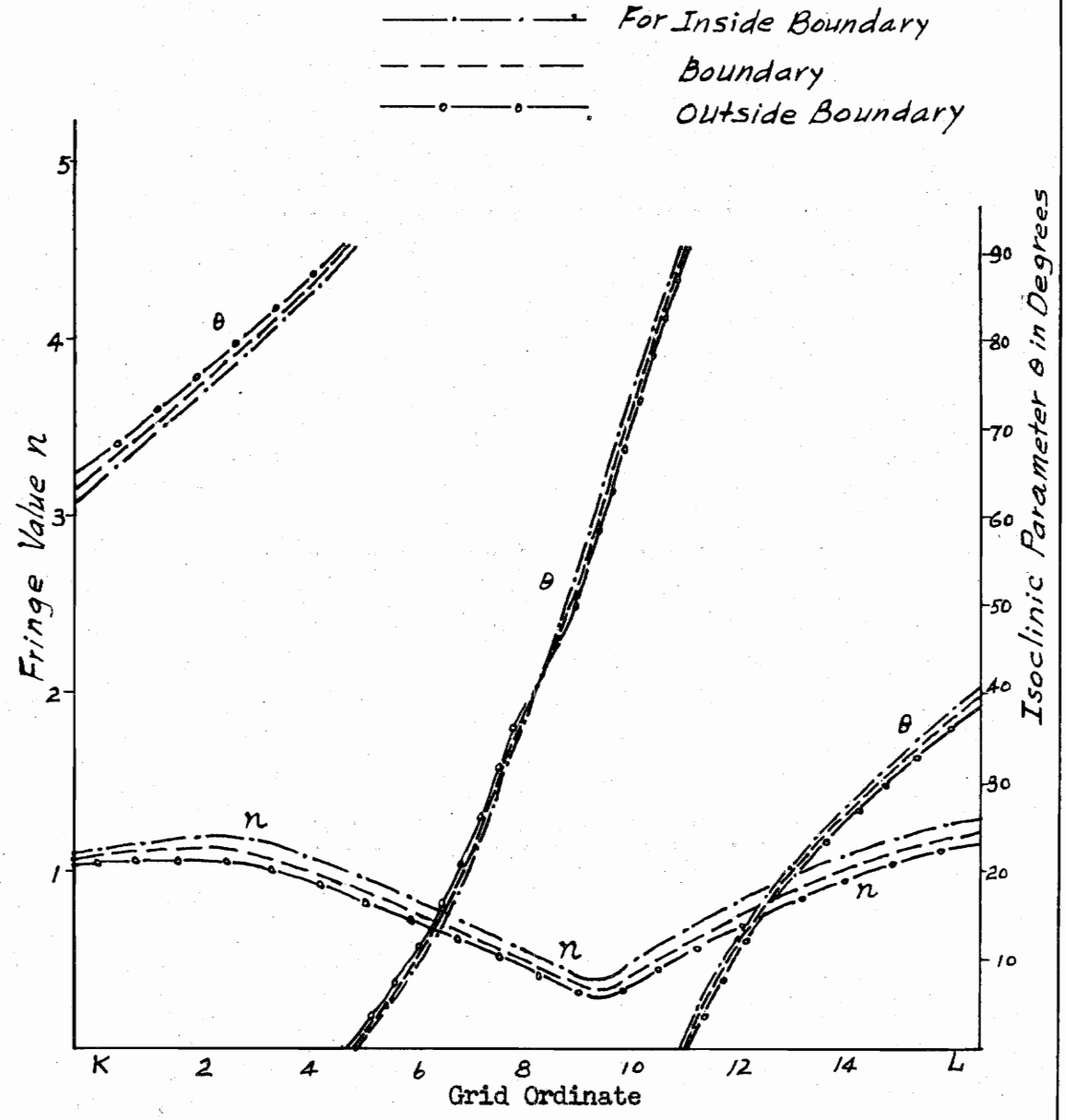

Fig. 25 - Curves of "n" and "θ"
Boundary KL

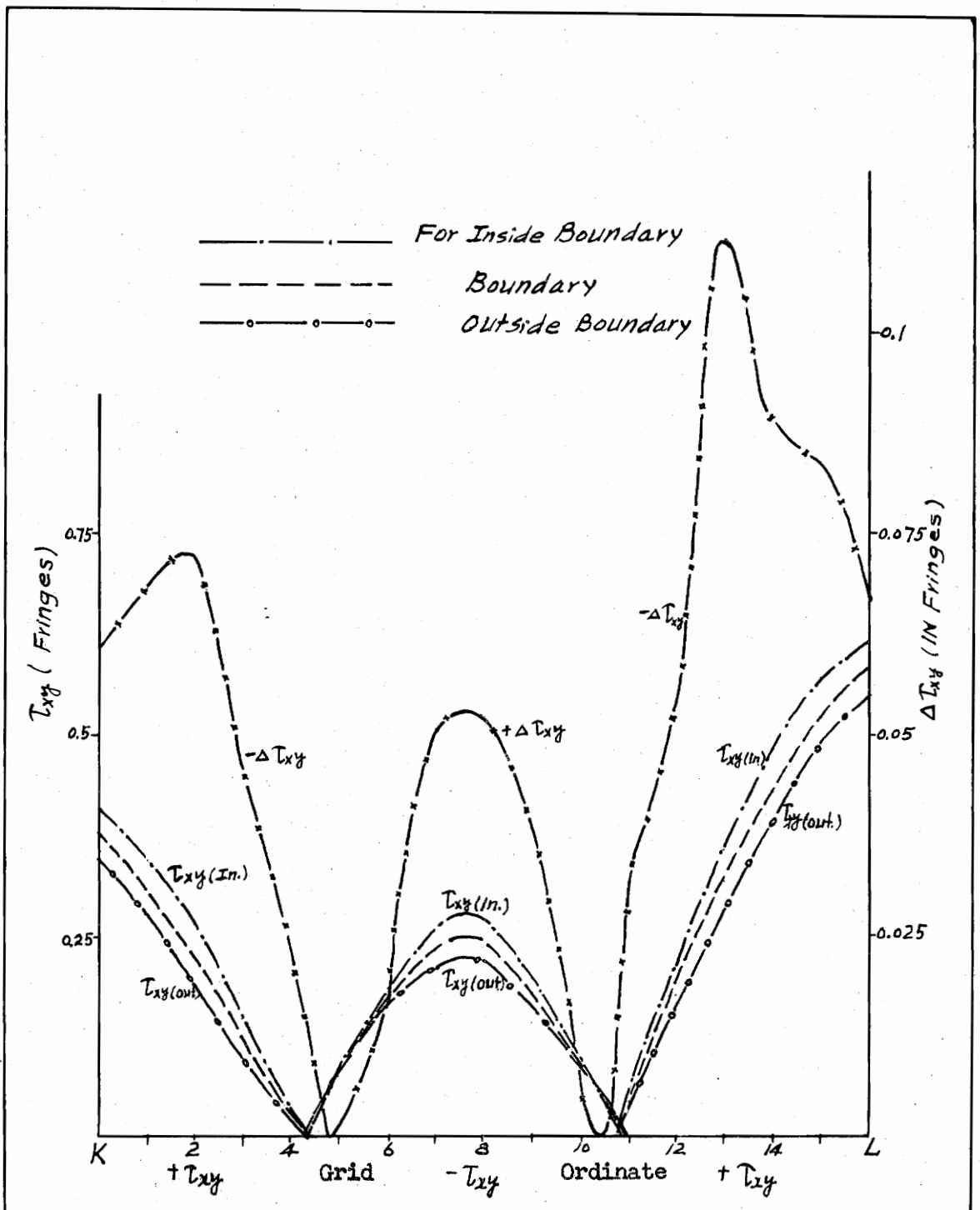

Fig. 26 - Curves of τ_{xy} and $\Delta\tau_{xy}$
Boundary KL

Table 17 Computation of σ_x

Boundary KL

Ord.	$\Delta\tau_{xy}$	$\frac{\Delta x}{\Delta y}$	$\sigma_{x(n-1)}$	$\sigma_{x(n)}$
K				-0.2563
1	-0.0680	-1	-0.2563	-0.3243
2	-0.0721	-1	-0.3243	-0.3964
3	-0.0462	-1	-0.3964	-0.4426
4	-0.0268	-1	-0.4426	-0.4694
5	0.0011	-1	-0.4964	-0.4683
6	0.0119	-1	-0.4683	-0.4564
7	0.0505	-1	-0.4564	-0.4059
8	0.0523	-1	-0.4059	-0.3536
9	0.0381	-1	-0.3536	-0.3155
10	0.0014	-1	-0.3155	-0.3141
11	-0.0307	-1	-0.3141	-0.3448
12	-0.0542	-1	-0.3448	-0.3990
13	-0.1122	-1	-0.3990	-0.5012
14	-0.0908	-1	-0.5012	-0.5920
15	-0.0838	-1	-0.5920	-0.6758
L	-0.0666	-1	-0.6758	-0.7424

Table 18 Computation of σ_y

Boundary KL

(1) Ord.	(2) (p-q)	(3) $(p-q)^2$	(4) τ_{xy}	(5) $4\tau_{xy}^2$	(6) (3-5)	(7) $\sqrt{6}$	(8) σ_x	(9) σ_y	(10) $\sigma_x > \sigma_y$ or $\sigma_y > \sigma_x$
K	1.10	1.2100	0.3774	0.5696	0.6404	0.8000	-0.2563	0.5437	$\sigma_y > \sigma_x$
1	1.12	1.2544	0.3077	0.3784	0.8760	0.9359	-0.3242	0.6116	
2	1.13	1.2769	0.2237	0.2000	1.0769	1.0345	-0.3964	0.6381	
3	1.07	1.1449	0.1233	0.0608	1.0841	1.0393	-0.4456	0.5967	
4	0.98	0.9604	0.0114	0.0004	0.9600	0.9797	-0.4694	0.5103	
5	0.86	0.7396	0.0709	0.0200	0.7196	0.8479	-0.4683	0.3796	
6	0.75	0.5625	0.1789	0.1280	0.4345	0.6588	-0.4564	0.2024	
7	0.61	0.3721	0.2353	0.2214	0.1507	0.3872	-0.4059	-0.0187	
8	0.50	0.2500	0.2477	0.2454	0.0046	0.0678	-0.3536	-0.2858	
9	0.36	0.1296	0.1672	0.1118	0.0178	0.1334	-0.3155	-0.4489	$\sigma_x > \sigma_y$
10	0.41	0.1681	0.0972	0.0377	0.1304	0.3605	-0.3141	-0.6746	
11	0.60	0.3600	0.0443	0.0076	0.3524	0.5932	-0.3448	-0.9380	
12	0.75	0.5625	0.1732	0.1196	0.4429	0.6655	-0.3990	-1.0645	
13	0.88	0.7744	0.3191	0.4072	0.3672	0.6058	-0.5012	-1.1070	
14	1.00	1.0000	0.4300	0.7396	0.2604	0.5099	-0.5920	-1.1019	
15	1.11	1.2321	0.5231	1.0946	0.1375	0.3701	-0.6758	-1.0459	
L	1.19	1.4161	0.5868	1.3772	0.0389	0.1972	-0.7424	-0.9396	

Table 19 Computation of $\sigma_x + \sigma_y = p + q$

Boundaries GK, KL, LH

Ord.	p+q	Corrected p+q	Ord.	p+q	Corrected p+q
G	2.5000	2.50	9	-0.7644	-0.94
5	1.0185	1.02	10	-0.9887	-1.17
6	0.7900	0.79	11	-1.2828	-1.38
7	0.6608	0.65	12	-1.4635	-1.57
8	0.5644	0.54	13	-1.6082	-1.73
9	0.4724	0.44	14	-1.6939	-1.87
10	0.3696	0.35	15	-1.7217	-1.95
K	0.2874	0.28	L	-1.6820	-2.04
1	0.2873	0.22	10	-1.9260	-2.12
2	0.2417	0.18	9	-1.8023	-2.18
3	0.1511	0.08	8	-2.1115	-2.22
4	0.0409	-0.04	7	-1.9621	-2.24
5	-0.0887	-0.17	6	-2.0282	-2.24
6	-0.2540	-0.34	5	-1.8820	-2.10
7	-0.4246	-0.54	H	-1.0828	-1.40
8	-0.6394	-0.72			

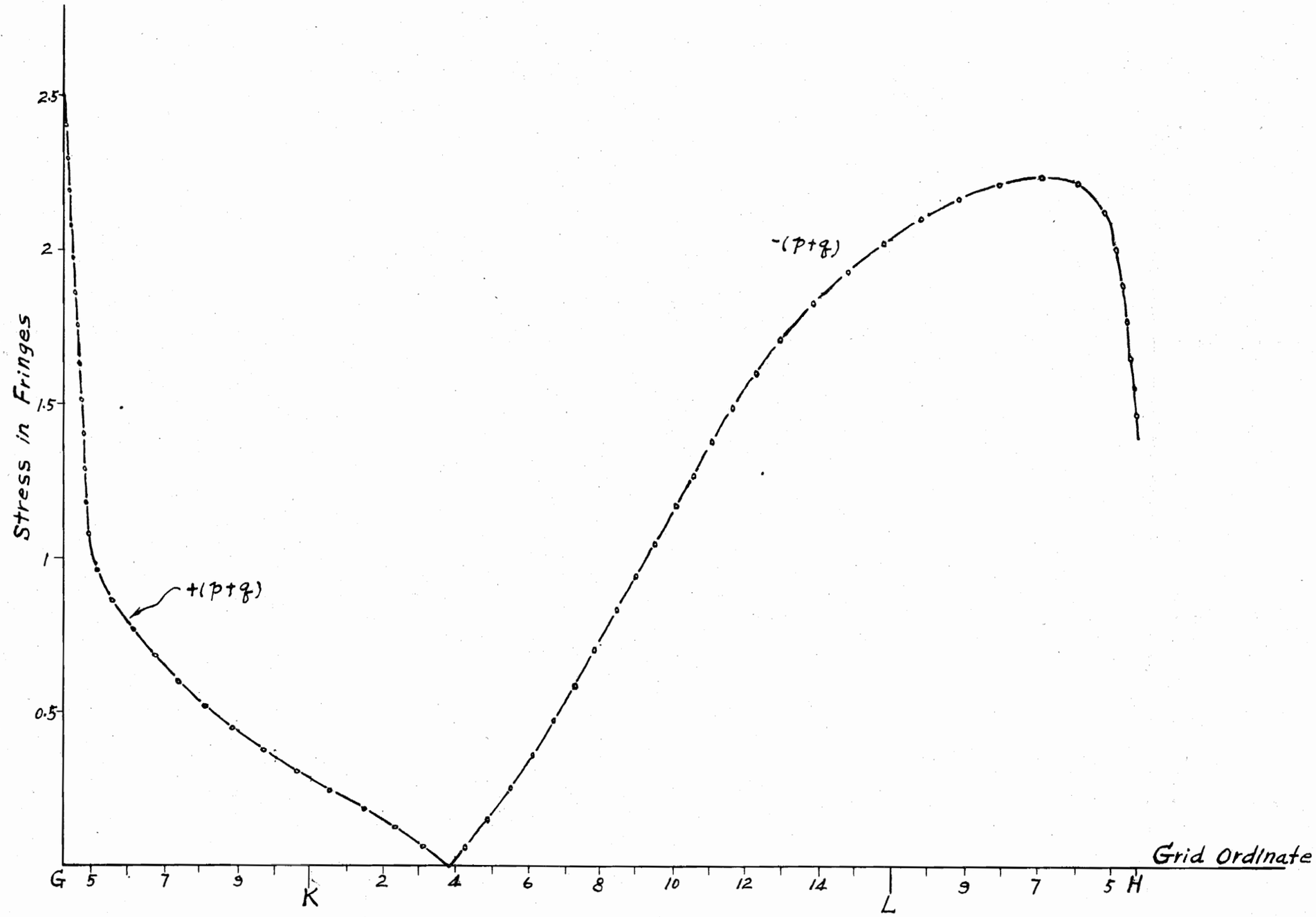

Fig. 27 Corrected p+q, Boundaries GK, KL, LH

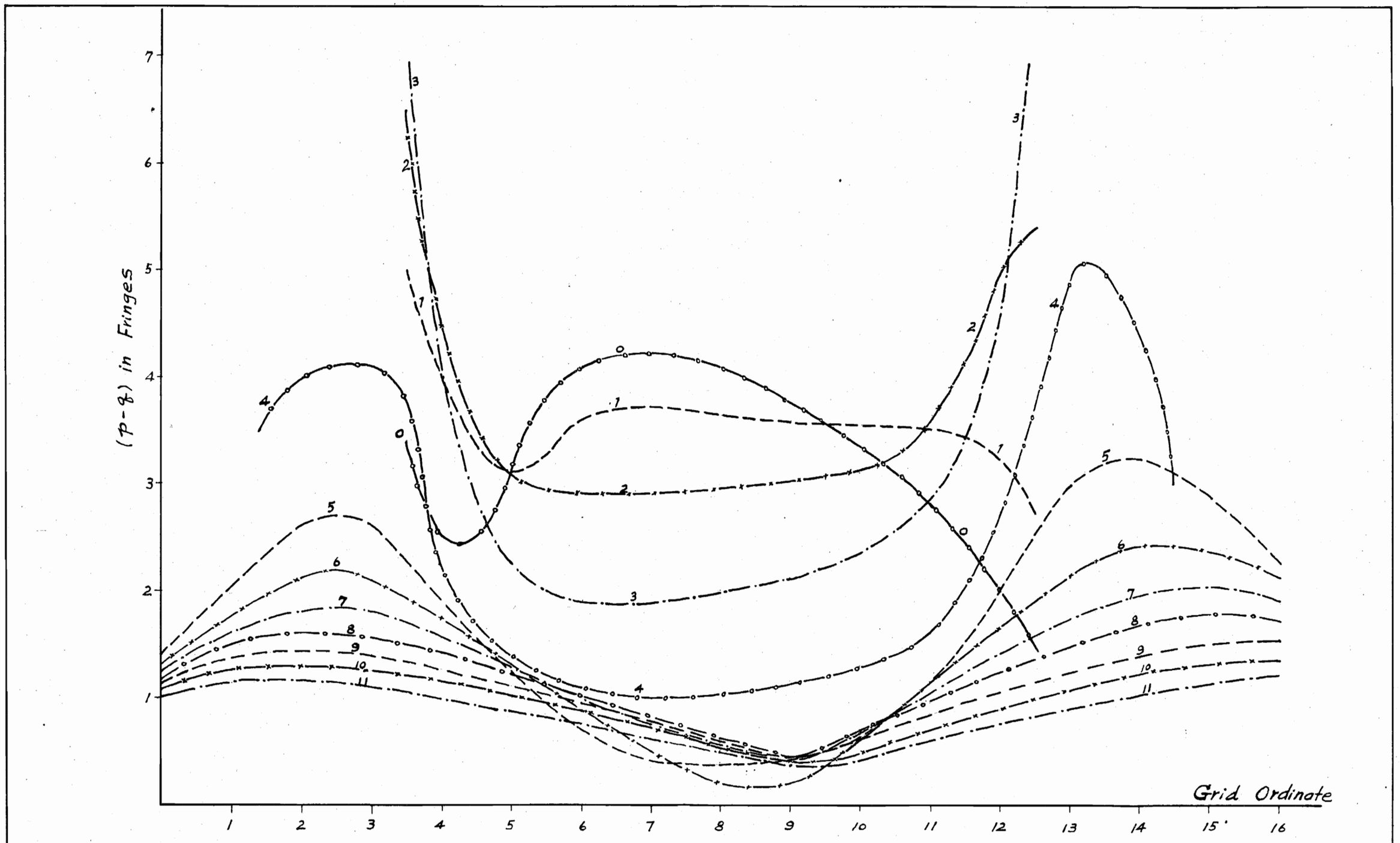

Fig. 28 - Curves of (P-Q) along lines Parallel to X-axis

Table 20 Influence Coefficientss

Point X - Y	Proportional Dimensions a	b	c	d	Influence Coefficient C_A	C_B	C_C	C_D	
4 - 10	15	15	5.5	15	0.196	0.134	0.535	0.134	0.999
4 - 9	15	15	6.5	15	0.210	0.151	0.486	0.151	0.998
4 - 8	15	15	11.0	15	0.244	0.211	0.332	0.211	0.998
3 - 7	15	11	15.0	15	0.211	0.332	0.211	0.244	0.998
2 - 7	15	3	8.0	15	0.094	0.606	0.177	0.121	0.998
1 - 6	15	13	15.0	15	0.232	0.286	0.232	0.248	0.998
12 - 10	5.0	15	15.0	15	0.562	0.125	0.187	0.125	0.999
12 - 9	5.5	15	15.0	15	0.535	0.134	0.196	0.134	0.999
12 - 8	9.0	15	15	15	0.390	0.187	0.234	0.187	0.998
13 - 7	15.0	9	15	15	0.187	0.390	0.187	0.234	0.998
14 - 7	6.0	2	15	15	0.178	0.661	0.071	0.088	0.998
15 - 6	15.0	13	15	15	0.232	0.286	0.232	0.248	0.998

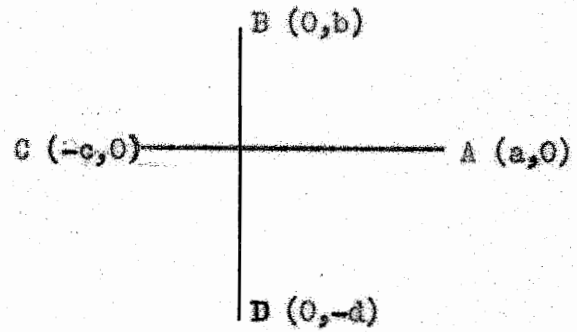

P+q (Fringes)	P (Fringes)
P-q (Fringes)	q (Fringes)

Y	0	1	2	3	4	5	6	7	8	9	10	11	12	13	14	15	16
0	+3.40	+2.34	+2.42	+1.30	+2.20	-0.50	+1.81	-1.15	+1.51	-1.80	+1.16	-1.55	+1.10	-1.68	+0.83	-2.05	+0.38	-1.92	+0.04	-1.40
	2.50	-0.08	3.10	-0.90	4.12	-2.31	4.18	-2.66	4.12	-2.96	3.76	-2.65	3.35	-2.51	2.82	-2.43	2.00	-1.96		
1	+5.00	+4.23	+4.11	+2.38	+2.74	+0.76	+2.18	-0.31	+1.70	-1.09	+1.28	-1.54	+1.03	-2.01	+0.77	-2.54	+0.48	-2.81	+0.22	-2.70
	4.00	+0.12	3.10	-0.36	3.60	-1.42	3.71	-2.01	3.66	-2.37	3.60	-2.57	3.55	-2.78	3.50	-3.02	3.25	-3.03		
2	+7.50	+5.82	+5.16	+3.26	+3.13	+1.48	+2.19	+0.22	+1.56	-0.72	+1.14	-1.50	+0.78	-2.31	+0.39	-3.31	+0.17	-4.70	+0.15	-5.40
	4.50	+0.66	3.00	+0.13	2.90	-0.71	2.90	-1.34	3.00	-1.86	3.07	-2.28	3.08	-2.70	3.66	-3.48	5.00	-4.85		
3	+8.50	+5.75	+4.87	+3.36	+2.76	+1.68	+1.79	+0.44	+1.19	-0.55	+0.72	-1.45	+0.33	-2.42	-0.03	-3.71	-0.45	-5.88	-0.56	-8.50
	4.00	+0.88	2.17	+0.60	1.90	-0.11	1.95	-0.75	2.00	-1.27	2.12	-1.78	2.36	-2.39	2.81	-3.26	4.75	-5.32		
4	+2.50	+3.00	+3.50	+4.21 4.00	+4.59 +4.10	+5.57	+4.83	+4.22	+3.20	+2.75	+2.06	+1.48	+1.28	+0.42	+0.71	-0.48	+0.28	-1.34	-0.09	-2.23	-0.47	-3.26	-0.83	-4.45	-0.95	-5.33	-0.16	-3.83	+0.23 -4.06	-7.50 -4.00	-3.00	-2.20	-1.40
					+0.11	4.10	+0.74	2.19	+1.02	1.37	+0.69	1.08	+0.20	1.00	-0.29	1.05	-0.76	1.15	-1.25	1.28	-1.76	1.60	-2.43	2.75	-3.60	5.00	-5.17	4.30						
5	+1.02	+1.21	+2.11	+2.03	+2.89	+2.74	+3.34	+2.97	+2.83	+2.34	+1.98	+1.61	+1.09	+0.88	+0.26	-0.30	-0.49	-0.04	-1.22	-0.38	-1.94	0.66	-2.68	-0.76	-3.34	-0.67	-3.65	-0.32	-3.14	+0.05	-2.43	+0.21	-2.10	+0.07
	1.40	-0.19	1.95	+0.08	2.60	+0.15	2.60	0.37	1.84	+0.49	1.25	+0.37	0.68	+0.21	0.35	-0.04	0.40	-0.45	0.45	-0.84	0.62	-1.28	1.15	-1.92	2.00	-2.67	3.00	-3.33	3.25	-3.19	2.86	-2.64	2.25	-2.17
6	+0.74	+1.02	+1.44	+1.59	+1.91	+2.01	+2.08	+2.09	+1.82	+1.77	+1.30	+1.30	+0.69	+0.78	+0.07	+0.28	-0.52	-0.16	-1.11	-0.45	-1.67	-0.52	-2.20	-0.52	-2.62	-0.50	-2.81	-0.34	-2.68	-0.13	-2.41	-0.02	-2.24	-0.06
	1.30	-0.28	1.75	-0.16	2.12	-0.10	2.10	-0.01	1.72	+0.05	1.30	+0	0.87	-0.09	0.50	-0.21	0.20	-0.36	0.20	-0.66	0.62	-1.15	1.15	-1.68	1.62	-2.12	2.12	-2.47	2.42	-2.55	2.36	-2.39	2.12	-2.18
7	+0.65	+0.93	+1.01	+1.30	+1.25	+1.53	+1.30	+1.54	+1.12	+1.33	+0.76	+1.01	+0.33	+0.64	-0.13	+0.31	-0.59	-0.04	-1.04	-0.32	-1.47	-0.38	-1.86	-0.42	-2.17	-0.38	-2.24	-0.29	-2.36	-0.20	-2.30	-0.14	-2.24	-0.17
	1.22	-0.28	1.60	-0.29	1.81	-0.28	1.79	-0.24	1.55	-0.21	1.27	-0.25	0.95	-0.31	0.75	-0.44	0.50	-0.55	0.40	-0.72	0.71	-1.09	1.02	-1.44	1.41	-1.79	1.75	-2.05	1.95	-2.16	2.02	-2.16	1.90	-2.07
8	+0.54	+0.84	+0.71	+1.10	+0.81	+1.20	+0.79	+1.17	+0.64	+1.01	+0.38	+0.79	+0.06	+0.53	-0.28	+0.24	-0.64	-0.03	-0.99	-0.27	-1.33	-0.31	-1.64	-0.35	-1.87	-0.34	-2.06	-0.30	-2.15	-0.24	-2.19	-0.21	-2.22	-0.26
	1.15	-0.30	1.50	-0.39	1.60	-0.39	1.55	-0.38	1.39	-0.37	1.20	-0.41	1.00	-0.47	0.77	-0.52	0.58	-0.61	0.44	-0.72	0.70	-1.02	0.94	-1.29	120	-1.55	1.46	-1.76	1.67	-1.91	1.76	-1.98	1.70	-1.96
9	+0.44	+0.77	+0.50	+0.93	+0.52	+0.87	0.46	+0.93	+0.32	+0.79	+0.11	+0.60	-0.13	+0.40	-0.41	+0.17	-0.69	-0.06	-0.97	-0.27	-1.25	-0.30	-1.50	-0.32	-1.72	-0.34	-1.89	-0.34	-2.01	-0.32	-2.09	-0.29	-2.18	-0.34
	1.1	-0.33	1.36	-0.43	1.42	-0.45	1.40	-0.47	1.26	-0.47	1.10	-0.49	0.94	-0.53	0.75	-0.58	0.57	-0.63	0.42	-0.70	0.65	-0.95	0.85	-1.18	1.03	-1.38	1.20	-1.55	1.37	-1.69	1.50	-1.80	1.50	-1.84
10	+0.35	+0.70	+0.35	+0.79	+0.32	+0.79	+0.24	+0.74	+0.10	+0.61	-0.06	+0.47	-0.26	+0.30	-0.48	+0.11	-0.71	-0.07	-0.95	-0.27	-1.20	-0.32	-1.42	-0.35	-1.62	-0.36	-1.79	-0.36	-1.92	-0.35	-2.02	-0.36	-2.12	-0.39
	1.05	-0.35	1.24	-0.44	1.26	-0.47	1.24	-0.50	1.13	-0.51	1.00	-0.53	0.86	-0.56	0.71	-0.59	0.56	-0.64	0.40	-0.68	0.55	-0.88	0.72	-1.07	0.89	-1.26	1.06	-1.43	1.22	-1.57	1.30	-1.66	1.34	-1.73
11	+0.28	+0.64	+0.22	+0.67	+0.18	+0.65	+0.08	+0.57	-0.04	+0.47	-0.17	+0.34	-0.34	+0.20	-0.54	+0.03	-0.72	-0.11	-0.94	-0.29	-1.17	-0.38	-1.38	-0.39	-1.57	-0.41	-1.73	-0.42	-1.87	-0.43	-1.95	-0.42	-2.04	-0.42
	1.00	-0.36	1.12	-0.45	1.13	-0.47	1.07	-0.49	0.98	-0.51	0.86	-0.51	0.75	-0.54	0.61	-0.57	0.50	-0.61	0.36	-0.65	0.41	-0.79	0.60	-0.99	0.75	-1.16	0.88	-1.31	1.00	-1.44	1.11	-1.53	1.19	-1.62
X	0	1	2	3	4	5	6	7	8	9	10	11	12	13	14	15	16																	

Fig. 29 - Final Result of Iteration and Computation

B. Calibration

Calibration for determining the material fringe constant was made with a tension bar, o.45 inch wide, 0.279 inch thick and 5 inch long. This bar was carefully machined on a bench milling machine. Adjustment for central loading was made so that the fringe appeared symmetrically from both sides of the central line of the specimen.

Due to the presence of the initial edge stress, the calibration curve as shown in Fig. 30 does not pass through the origin. This, however, will not have an appreciable effect on the value of the fringe constant.

The material fringe constant, f, was obtained from the equation (see Handbook of Experimental Stress Analysis by M. Hetenyi, p. 867, John Wiley & Sons, 1950):

$$f = \frac{P}{bn}$$

where P = The applied load, lb.

b = The width of specimen, in.

n = The fringe order

From the data in Fig. 30,

$$f = \frac{378 - 48}{0.45 \times 8} = 91.6 \text{ lb./in./fringe}$$

Compared to the common average value of the fringe constant (86 lb./in./fringe) for this kind of material, the value of f obtained here is a little higher.

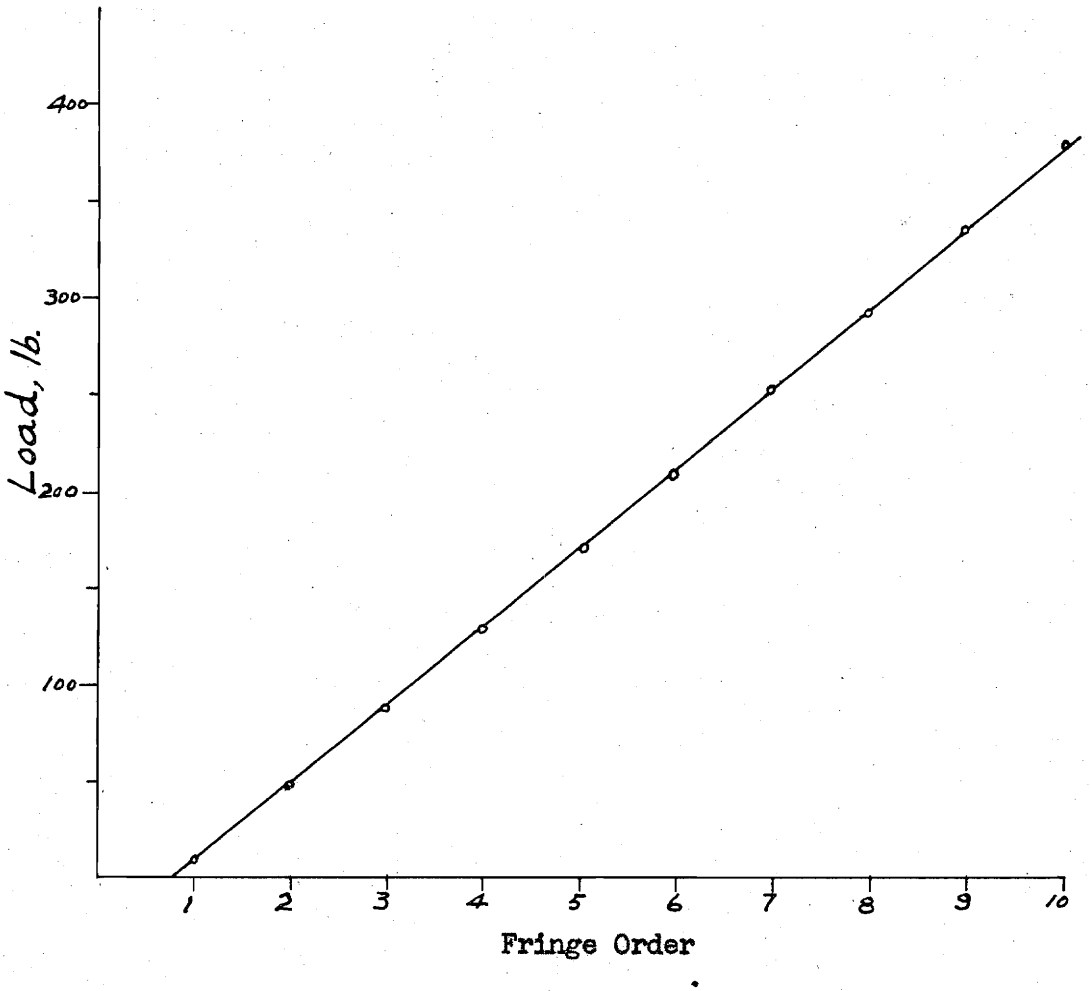

Fig. 30 - Calibration for Fringe Constant

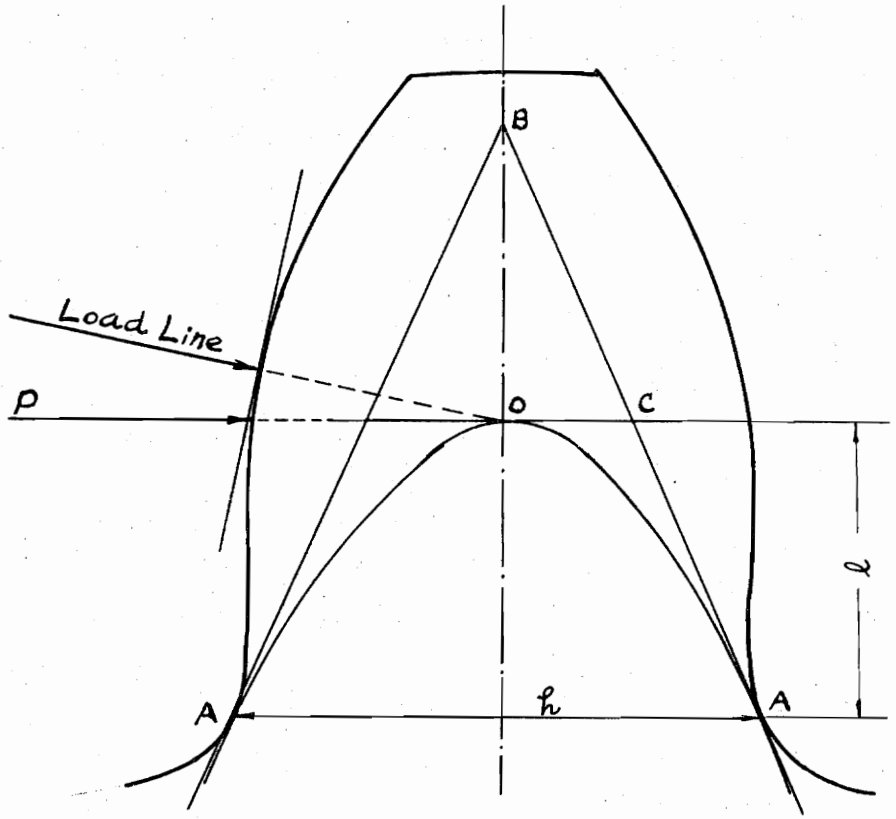

1 Extend the load line until it intersects the center line of the tooth at O.

2 Through O draw OC perpendicular to the center line of the tooth.

3 By means of a scale which is kept tangent to the tooth profile near the fillet, draw a line such that AC = BC. Then section AA is the critical section.

4 By measuring, h = 2.7 inch, = 1.55 inch.
On actual gear, h = 0.412", = 0.237" (divided by the magnification 6.54)

Fig. 31 - Determination of the Critical Section for Lewis' Formula

C. Calculation of the Stress Concentration Factor

The stress concentration factor K is defined as

$$K = \frac{\sigma_1}{\sigma_2}$$

where σ_1 = Tensile stress at the critical section as obtained from the photoelastic stress pattern.

σ_2 = Tensile stress at the critical section as calculated from Lewis' formula.

a. Tensile Stress σ_1

$$\sigma_1 = \frac{fn}{t}$$

where t = Thickness of the gear model = 0.279 inch.

f = The fringe constant = 91.2 lb./inch/fringe.

n = The fringe order = 8.5 fringes.

hence $$\sigma_1 = \frac{91.2 \times 8.5}{0.279} = \frac{775.2}{0.279} = 2,778.5 \text{ psi}$$

b. Tensile Stress σ_2

$$\sigma_2 = \frac{6Pl}{bh^2}$$

From Fig. 31, P = 55 lbs.

= 0.237 inch.

h = 0.412 inch.

b = 0.279 inch = Thickness of the model.

hence $$\sigma_2 = \frac{6 \times 55 \times 0.237}{0.279 \times 0.412^2} = 1,650 \text{ psi}$$

c. The Concentration factor K

$$K = \frac{2778.5}{1650} = 1.68$$

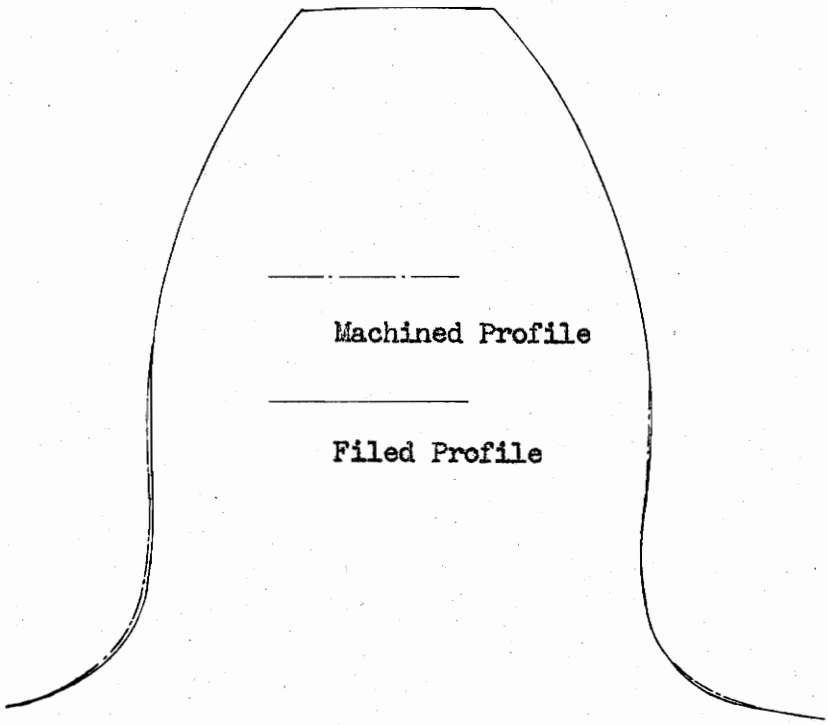

Fig. 32 - Comparison of the Profiles of teeth made by filing and by machining

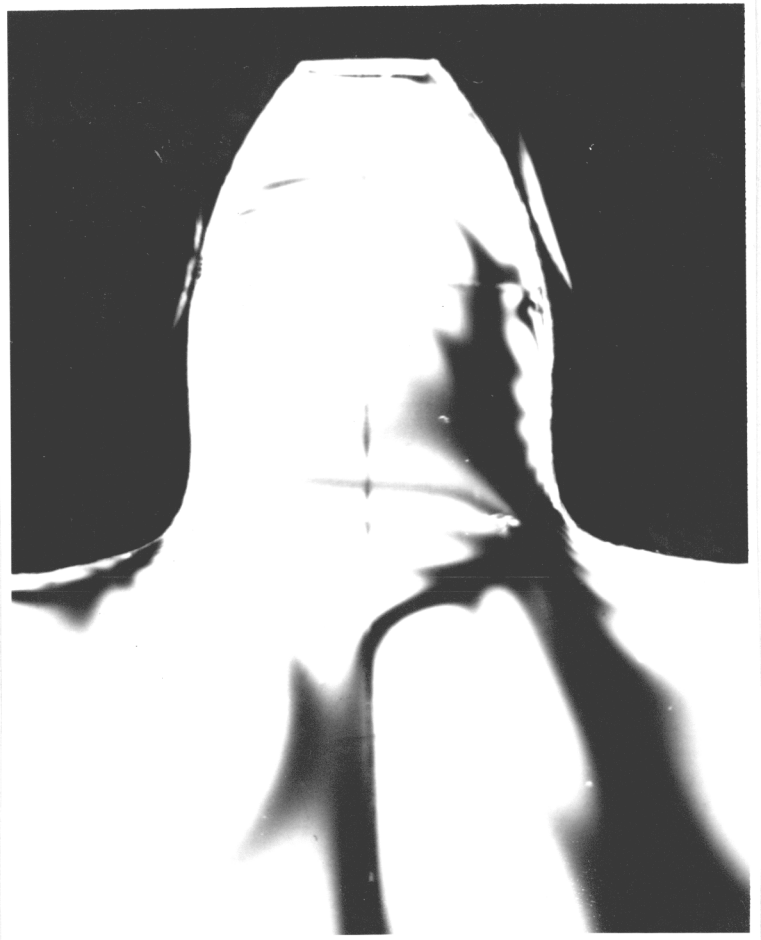

Isoclinics, 30 Degrees

Isoclinics, 50 Degrees

Fig. 33 - Isoclinics

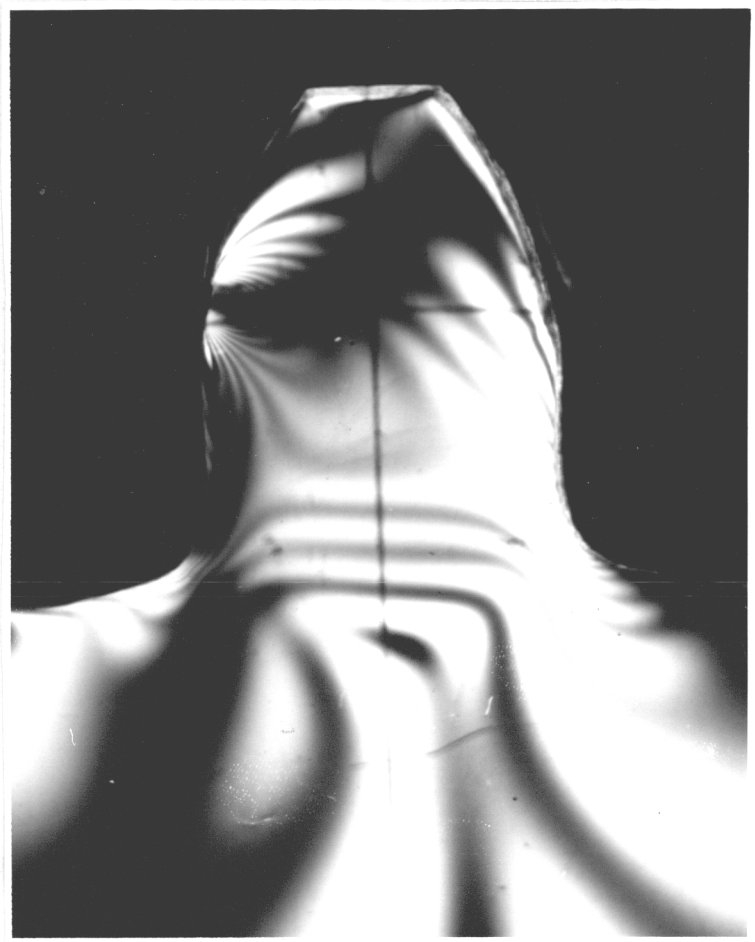

Isoclinics, 70 Degrees

Isoclinics, 90 Degrees

Fig. 34 - Isoclinics

X. ACKNOWLEDGMENT

The author is deeply indebted to Dr. E. D. Harrison for his continued interest and guidance during this investigation.

The author also wishes to express his heartfelt gratitude and appreciation to Prof. J. B. Jones for giving him the opportunity to undertake this investigation, to Profs. D. H. Pletta, Dan Frederick, and C. E. Trent for their valuable suggestions and corrections, to Prof. H. L. Woods for his generous loan of the gear-loading apparatus and to Mr. G. K. McCauley for his skillful and untiring assistance in making the model and photographs.

XI. BIBLIOGRAPHY

1. MacGregor, C. W., "Mechanical Properties of Materials", Handbook of Experimental Stress Analysis, Chapter 1, p. 25, John Wiley & Sons, 1950.

2. Lewis, Wilfred, "Investigation of the Strength of Gear Teeth", Proc. Engineer's Club of Philadelphia, 1893.

3. Coker, E. G., "Engineering Problems solved by Photoelastic Methods", Journal of the Franklin Institute, 1923.

4. Timoshenko, S. and Baud, R. V., "The Strength of Gear Teeth", Mechanical Engineering, Vil. 48, p. 1,105, Nov., 1926.

5. Baud, R. V. and Peterson, R. E., "Load and Stress Cycles in Gear Teeth", Mechanical Engineering, Vol. 51, p. 653, 1929.

6. Black, P. H., "An Investigation of Relative Stresses in Solid Spur Gears by the Photoelastic Method", University of Illinois Engineering Experiment Station, Bulletin No. 288, Dec., 1936.

7. Dolan, T. J. and Broghamer, E. L., "A Photoelastic Study of Stresses in Gear Tooth Fillets", University of Illinois Engineering Experiment Station, Bulletin No. 335, 1942.

8. Harrison, E. D., "The Separation of the Principal Stresses at the Base of a Gear Tooth", Purdue Thesis, 1952.

XII. VITA

The author was born on Nov. 9, 1924 in Anhwei, China. He was graduated from the National 9th High School, Szechwan, China in 1942. He received the B. S. degree from the Ordnance Engineering College, Chungking, China in 1947. Since that time, he worked in Chinese arsenals until he came to the United States in 1953. He is now engaged in graduate study in the Mechanical Engineering Department of the Virginia Polytechnic Institute, Blacksburg, Virginia.

K. C. Wang